

GNSS time series and velocities about a slowly convergent margin processed on HPC clusters: products and robustness evaluation

Lavinia Tunini¹, Andrea Magrin¹, Giuliana Rossi¹, David Zuliani¹

¹National Institute of Oceanography and Applied Geophysics - OGS, Trieste-Udine, Italy

Correspondence to: Lavinia Tunini (ltunini@ogs.it)

Abstract. Global Navigation Satellite Systems are well-known and fundamental tools for crustal monitoring projects and tectonic studies, thanks to ~~the~~their high coverage and the high-quality of the data- they provide. In ~~slow~~particular, at slowly convergent margins, ~~in particular,~~ where ~~the~~ deformation rates are of the order of a few mm/yr, ~~the~~ GNSS monitoring is proves to be beneficial to detect in detecting the ~~diffused~~diffuse deformation ~~which is~~ responsible for ~~the~~ tectonic stress accrual. Its strength is lies in the high precision ~~reached~~achieved by GNSS permanent stations, ~~particularly if especially when~~ long ~~span-~~term data and stable monuments are available at ~~all~~ the stations. North-East Italy ~~is a region which can take the most from continuous and high-precision geodetic monitoring, since it~~ is a tectonically active region located in the northernmost sector of the Adria microplate, slowly converging with the Eurasia plate, ~~but~~ characterised by low deformation rates and moderate seismicity. ~~Furthermore, this region is~~ It greatly benefits from continuous and high-precision geodetic monitoring, since it has been equipped with a permanent GNSS network providing real-time data and daily observations over two decades. The Friuli Venezia Giulia Deformation Network (FReDNet) was established in the area in 2002 to monitor crustal deformation and contribute to the regional seismic hazard assessment. This paper describes GNSS time series spanning two decades of stations located in the NE-Italy and surroundings, as well as the outcoming velocity field. The documented dataset has been retrieved by processing the GNSS observations with the GAMIT/GLOBK software ver10.71, which allows calculating high-precision coordinate time series, position and velocity for each GNSS station, and by taking advantage of the high-performance computing resources of the Italian High-Performance Computing Centre (CINECA) clusters.

The GNSS observations (raw and standard RINEX formats) and the time series estimated with the same procedure are currently daily continued, collected and stored in the framework of a long-term monitoring project. Instead, velocity solutions are planned to be updated annually. The time series and velocity field dataset documented here is available ~~at~~ <https://doi.org/10.13120/b6aj-2s32-on-Zenodo> (DOI 10.5281/zenodo.8055800) (Tunini et al., 2023).

1 Introduction

The Global Navigation Satellite ~~Systems~~System (GNSS) ~~provide~~allows obtaining a globally-extended positioning dataset which is a milestone essential not only for crustal deformation and tectonic studies but also for plenty of applications going from surveying to metrology and hazard monitoring projects in the environmental sciences. In recent years, the GNSS

31 technologysystem has been continuously and rapidly growing, with multi-constellation and multi-frequency signals supported
32 by cutting-edge processing algorithms devoted to the integration of different sensors (sensor fusion techniques) and
33 improvements in error mitigation procedures. The well-known GPS, combined with GLONASS and the more recent Galileo
34 and Beidou constellations, can provide velocity estimates of the position of a GNSS sensorstations with a precision that
35 reaches a few millimetres if precisions less than 1 mm/yr when long span data time-series, precise satellite orbits, and stable
36 monuments are available at the stations ~~are available~~.



37
38 **Fig. 1:** Map of the study area, with topography from ETOPO1 (Amante and Eakins, 2009). Red lines indicate the boundary of the
39 Adria microplate; we refer to the “Adria microplate” as the Adriatic sea plate domain, also including the Apulia block in the
40 southern Adriatic sea. Continental lithosphere polygons from GPlates 2.1 dataset (<https://www.earthbyte.org/gplates-2-1-software->

41 and-data-sets/ are in agreement with [Matthews et al. \(2016\)](#). AL: Albania; AS: Adriatic Sea; AU: Austria; CR: Croatia; EA:
42 Eastern Alps; NEI: North-East Italy; SL: Slovenia.

43

44 Notwithstanding the availability of reliable and consistent GNSS solutions at the global sealesscale, such as ~~e.g. the ones~~
45 those provided by the Nevada geodeticGeodetic Laboratory ([NGL](http://geodesy.unr.edu/)) (<http://geodesy.unr.edu/>; [Blewitt et al., 2018](#)), at the
46 regional sealesscale, it ~~can~~may be preferableuseful to consider an ad-hoc reference frame and to ~~then~~customise the processing
47 scheme, in order to obtain high-quality time series and high-quality velocity field in regions of particular interest. North-East
48 Italy (Fig. 1) is a particularly suitable region, ~~since a high~~because of the large number of GNSS stations ~~from~~deployed there
49 by different agencies ~~have been deployed since the early 2000s~~ to monitor the deformations ~~since the beginning of the century~~.
50 North-East Italy lies at the northern edge of the Adria microplate, a continental lithosphere block, part of the distributed
51 deformation zone between the African and Eurasian plates, encompassing the eastern Italian peninsula from Sicily to the
52 border with Austria and Slovenia, and the eastern Adriatic coast from Slovenia to Croatia and Albania ([Battaglia et al., 2003](#)).
53 Adria microplate is recognized to have a counterclockwise motion, implying its collision with Eurasia along its northern tip
54 ([Battaglia et al., 2003](#); [D'Agostino et al., 2005, 2008](#); [Serpelloni et al., 2005](#)). The convergence between Adria and Eurasia
55 plates leads to significant consequences on the deformation of the NE-Italy, as revealed by the moderate seismicity, primarily
56 concentrated in the southern sector of the Eastern Alps, and diffused tectonic deformation ([Castellarin and Cantelli, 2000](#);
57 [Bressan et al., 2021](#)). Although the deformation rates (2–3 mm/yr of N-S shortening; [D'Agostino et al., 2005](#); [Weber et al.,](#)
58 [2010](#); [Devoti et al., 2011](#)) remain quite low; if compared to fast converging margins like India-Eurasia or Arabia-Eurasia, this
59 is the most seismic active area of the entire Alps chain. Hence, ~~North-East~~northeastern Italy is ~~essential in a~~ key region for the
60 understanding of the Adria Plate geodynamics ([Brancolini et al., 2019](#); [Magrin and Rossi, 2020](#)). The deformation in the area
61 is currently monitored through GNSS instruments by the National Institute of Oceanography and Applied Geophysics - OGS,
62 the Friuli Venezia Giulia regional council and other entities, providing new and denser data to the information available since
63 the 60s of the ~~XX~~20th century from the NE-Italy subsurface tilt and strainmeter network ([Braitenberg and Zadro, 1999](#), [Rossi](#)
64 [et al., 2021](#)). The Friuli Venezia Giulia Deformation Network (FReDNet) is the GNSS network ~~installed~~established by the
65 OGS to monitor the distribution of the crustal deformation ~~distribution of~~ and provide supplementary information for the
66 regional earthquake hazard assessment ([Zuliani et al., 2018](#)). It ~~is~~ currently ~~counting~~includes 22 permanent GNSS stations
67 ~~providing data on the scale~~located at distances of 15-20 km from each other in most parts of the region ~~and covering a, most~~
68 of which have been in operation for more than 15 years ~~long period for the majority of the stations~~ (more details in Appendix
69 A). FReDNet is part of the ~~North-East Italy-OGS~~ seismic and geodetic monitoring system for the North-East Italy (Sistema
70 di Monitoraggio terrestre dell'Italia Nord Orientale - SMINO) ~~of OGS,~~ which also includes seismic broad-band and short
71 and mean period stations, as well as strong motion stations ([Bragato et al., 2021](#) and references therein).

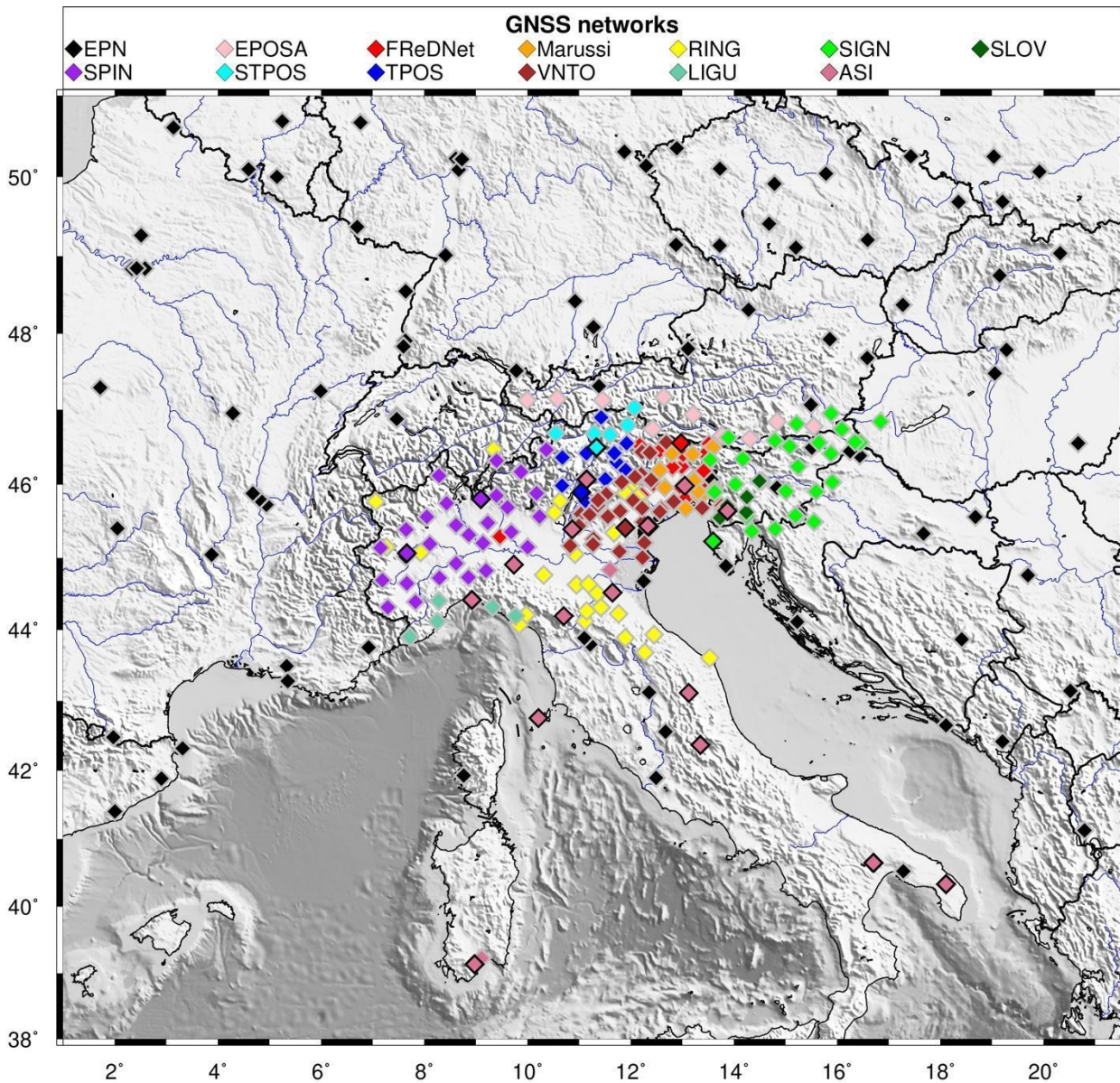
72 In this paper, we document a dataset of ~~coordinate~~position time series, ~~positions~~ and velocities for 350 stations in NE-Italy
73 and surroundings, whose data have been continuously collected over the past two decades. The dataset has the potential to
74 provide high-quality and updated information relative to an active but slow converging margin. Data have been processed

75 taking advantage of the high-performance computing resources offered by CINECA (<https://www.hpc.cineca.it/>) clusters
76 through the Italian SuperComputing Resource Allocation - ISCRA initiative, and through the resources available inside the
77 HPC Training and Research for Earth Sciences (HPC-TRES) program, co-sponsored by the Minister of Education, University
78 and Research (MIUR). The HPC-TRES training program, drown-up by OGS and CINECA, is targeted to promote advanced
79 training in the fields of Earth System sciences and enhance human resources and capacity building through the use of national
80 and European HPC infrastructures and services in the framework of the international infrastructure PRACE - The Partnership
81 for Advanced Computing in Europe (<https://prace-ri.eu/>). In Section 2 and in Section 3, we describe the collected input data
82 and the elaboration ~~procedure~~procedures, respectively. ~~Finally, the~~The dataset of time series and velocities is presented in
83 Section 4, whereas Section 5 illustrates some experiments to evaluate the dataset's quality and robustness. Section 6 provides
84 information on the data availability and Section 7 outlines some final considerations.

~~The dataset has the potential to provide high quality and updated information relative to an active but slow converging margin.
86 The elaboration procedure required to produce the dataset has been designed and performed by taking into consideration and
87 eventually correcting each slight bias or parameter selection error which can compromise the quality of the results and/or
88 cause a deviation of the small velocities estimated.~~

89 2 Input data

90 We considered the data recorded by all available permanent GNSS stations located in North-East Italy and surrounding
91 regions (Fig. 2). These stations belong to different networks: the OGS geodetic network FReDNet (<http://frednet.crs.ogs.it/>);
92 the GNSS network Antonio Marussi of the Friuli Venezia Giulia (FVG) regional council; ~~(Marussi)~~, with stations located
93 throughout the FVG region, ~~hence enhancing that enhance~~ the coverage offered by FReDNet ~~sites (Marussi)~~; the Veneto
94 region GPS network (VNTO); the Servizio di Posizionamento SPIN3 GNSS (SPIN), which is a network covering Lombardia,
95 Piemonte and Valle D'Aosta regions; the South Tyrolean Positioning Service (STPOS) and Trentino POSitioning Service
96 (TPOS), which are the geodetic networks of the Autonomous Provinces of Trento and Bolzano, respectively; the Liguria
97 region GNSS network (LIGU); the Rete Nazionale Integrata GNSS (RING) belonging to the National Institute of Geophysics
98 and Volcanology (INGV); the Nuova Rete Fiduciale Nazionale GNSS of the Italian Space Agency (ASI); the European
99 EUREF Permanent Network (EPN), which includes stations managed by different institutions; the Echtzeit Positionierung
100 Austria (EPOSA) network; the SIGNAL network of the Geodetic Institute of Slovenia (SIGN) and other Slovenian GNSS
101 sitesstations acquired by OGS in agreement with the University of Ljubljana and the non-profit organisation Zavod MPRI,
102 raziskovalna in razvojna dejavnost (previously with the Slovenian company Harphasea) (in the following: SLO_GPS).
103 Although some of these networks were designed for cadastral and civil purposes, the validity of such data for velocity
104 estimates has been demonstrated in several works since the benefit of redundancy and increased spatial density overcomes
105 the noise eventually present (Serpelloni et al., 2022 and references therein).



107

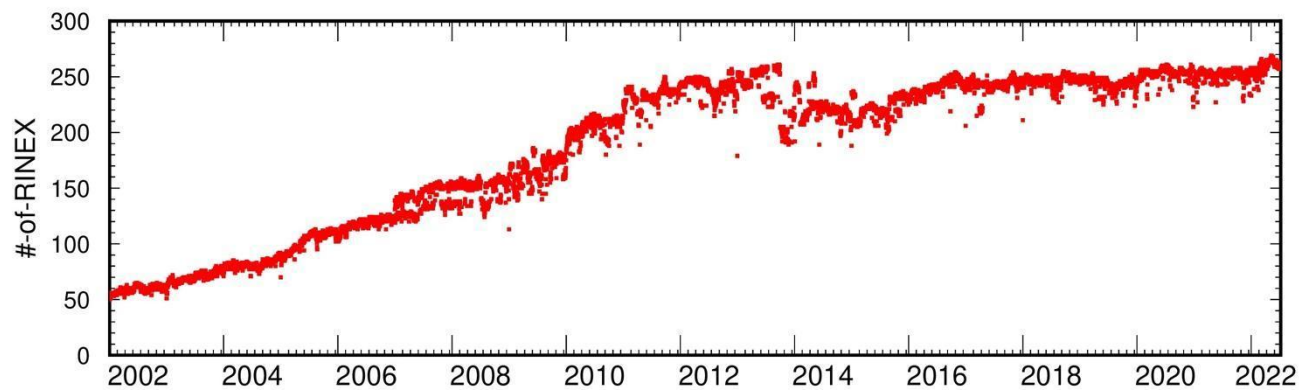
108 **Fig 2: GNSS stations location and belonging network-networks. Different colours stand for different networks, as indicated in the**
 109 **legend (see main text for the abbreviations). Symbols contoured by black lines indicate thethose stations which belong belonging**
 110 **to both a regional network but also and to the European network EPN. In the legenda the explanation of the colours used for the**
 111 **different networks (see the text for the abbreviations).⌘**

112

113 In order to link our solutions to the international reference frame International Terrestrial Reference Frame ITRF14, (Altamimi
 114 et al., 2016), we also consider the data coming from reference stations/sites belonging to the EPN and the International GNSS

115 [Service \(IGS, https://igs.org/data/\)](https://igs.org/data/) networks. In a rectangular area ~~going extending~~ from 39.75°N to 50.70°N latitude and from
116 1.5° to 21°E longitude and centred in N-E Italy, whose size has been empirically selected to obtain a stable position-velocity
117 solution for each of the target stations, we consider as reference ~~stationssites~~ all the EPN and IGS sites located inside it,
118 ~~addingwith~~ four ~~moreadditional~~ EPN sites located in Sardinia (CAGL, CAG1, CAGZ and UCAG) ~~added~~ to improve the
119 coverage in the southern sector. ~~Although we consider~~ While our study encompasses more than 350 stations ~~insidewithin~~ the
120 ~~studydesignated~~ area ~~overall in this work~~ (5 stations - GUMM, LECC, LEIB, RUDI, SILL - were moved more than 1 m from
121 the original position; therefore, we renamed them), the ~~numberactual volume~~ of data ~~available~~ is ~~sensibly inferior,~~
122 ~~progressively increasing~~ considerably lower. It has shown a progressive increase, starting from ~~somejust a few~~ tens of data/
123 ~~per day available~~ in 2002, to ~~reaching~~ approximately 250 data/~~points per day available since in~~ 2011 (Fig. 3). ~~The drop in~~
124 ~~the number of stations since 2013 is due to a sudden restriction of the access to several stations located in Slovenia.~~ The data
125 availability highly depends on station operability, remote connection functioning, and decommissioning/installation of
126 stations.

127 The total number of the daily observation files processed in this study is about 0.57 million.
128



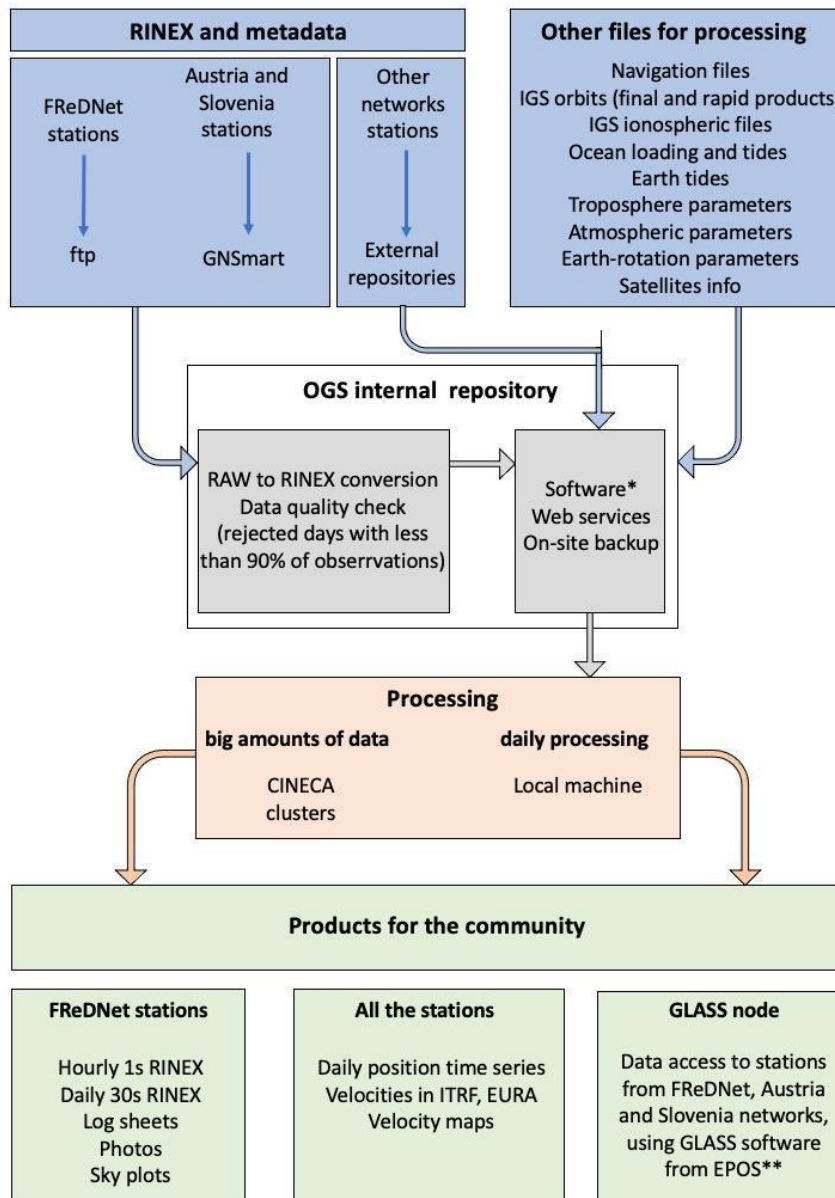
129
130 **Fig. 3: Amount of data available with time.**

131
132 We have collected GNSS observation data since 2002, 1st January. Raw data from the FReDNet network are collected,
133 quality-checked, transformed into the Receiver INdependent EXchange (RINEX) format, and then released, through a public
134 ftp repository, as hourly and daily files at both 1s and 30s sampling. Data from EPOSA network and SLO_GPS stations are
135 collected in real-time through the GNSMART software (Gerhard et al., 2001) and then converted into RINEX format for
136 post-processing. Finally, RINEX-formatted data deriving from the other networks are collected using different services of
137 data distribution: public data repository of the networks, EPN data distribution services and European Plate Observation
138 System (EPOS) service (Fig. 4).

139 Like the SMINO monitoring system to which it belongs, the FReDNet network aims to provide a monitoring service on a
140 long-term basis. Hence, raw observations and RINEX-formatted data from FReDNet stations are currently continuously
141 retrieved, collected and stored in the OGS internal repository on hourly and daily basis (FReDNet Data Centre, FReDNet DC
142 2016), where also real-time observations are available. FReDNet data are distributed under a Creative Common licence (CC
143 BY-SA) and accessible at the link <https://frednet.crs.ogs.it/DOI/>. They are allocated into folders according to the sampling
144 interval (~~RINEX 30s or RINEX 1s, for 30 seconds or 1 second sampled observations, respectively~~), ~~year~~ and ~~day of~~ the
145 ~~year (day)~~ date of the acquisition. From the same web page <https://frednet.crs.ogs.it/DOI/>, metadata of FReDNet sites
146 are also retrievable by clicking on the “~~log sheets~~ sitclogs” link.

147

148



149

150 Fig. 4: GNSS data flow at the OGS (Italy). *Software used: GAMIT/GLOBK ver10.71 (Herring et al., 2018) for GNSS data
 151 processing, GMT ver6.4.0 for plots and maps, GNSMART for downloading raw streams data from Austria and Slovenia networks
 152 and transform them into RINEX format data, TEQC (Estey and Meertens, 1999) for data quality check (it is end-of-life, but for
 153 GPS data it is still functional), Git ver2.27, free and open source system (<https://git-scm.com/>), for scripts updating and management
 154 between different machines, Anubis ver2.3 (<https://gnutsoftware.com/software/anubis>) for sky plots and RINEX3 generation. **
 155 <https://glass.gnss-epos.eu/#/site>

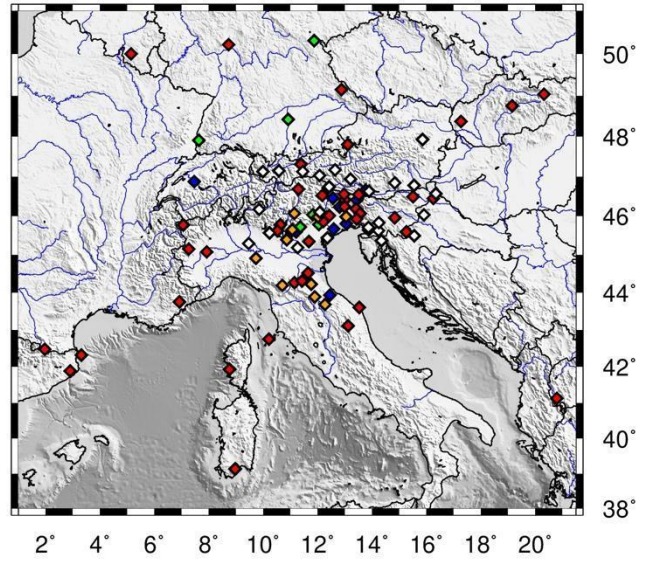
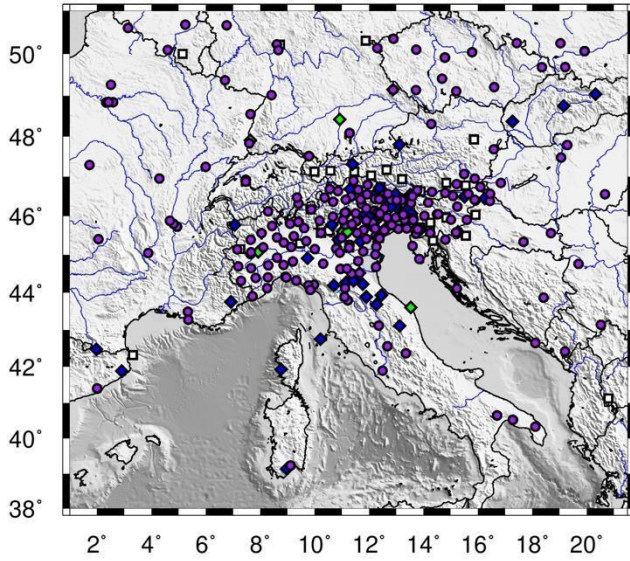
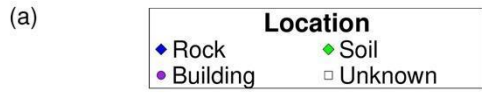
156

157 Along with the data, ~~log sheets~~sitelogs containing station metadata (e.g. station location, monument type, terrain description,
158 photos, etc.) are collected for each GNSS station. The primary information source for metadata are the log sheets in IGS
159 format (<https://www.igs.org/formats-and-standards/>) recovered through the public repository of each networks and from the
160 “Metadata Management and distribution system for Multiple GNSS Networks” (M3G) (<https://gnss-metadata.eu/site/index>).
161 If the network does not provide IGS ~~log sheets~~sitelogs, we extract the information from RINEX files header. Finally, we
162 verify the compatibility among different sources of metadata, when available.

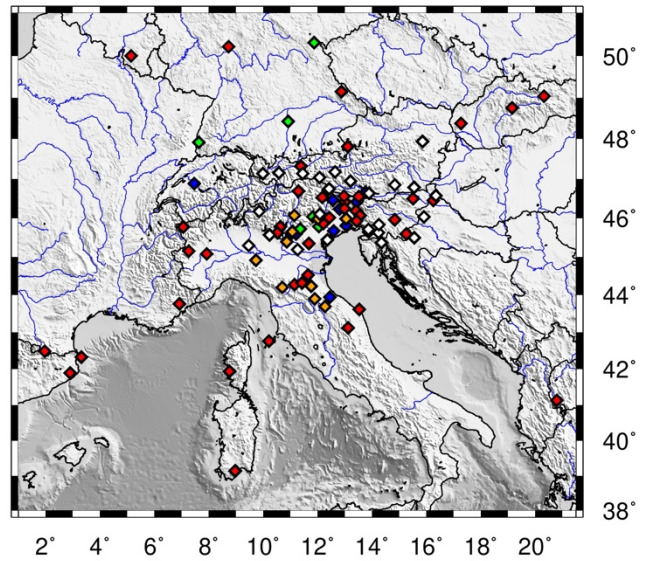
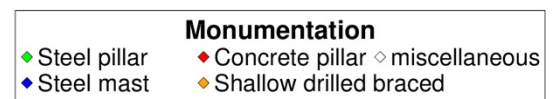
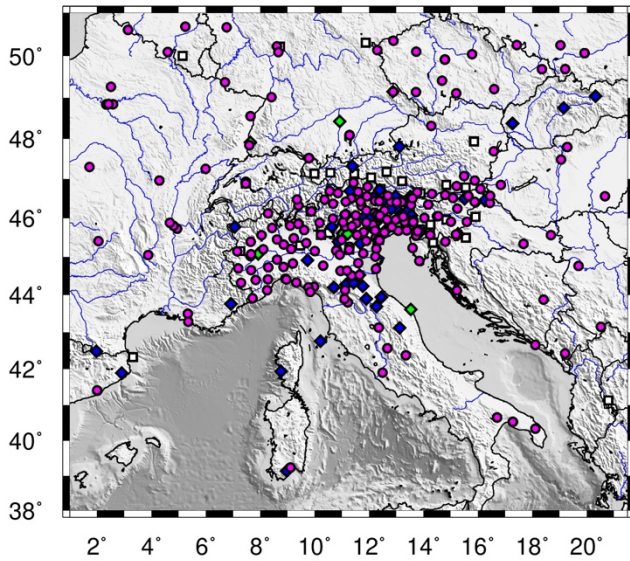
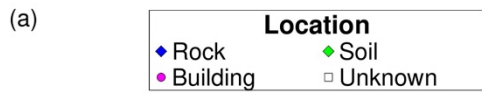
163 ~~Piece of information retrieved from the metadata is~~Metadata describes the history of the equipment, which is useful for
164 ~~identifying~~classifying discontinuities/~~jumps on in~~ the time series. ~~For the a priori coordinates of the stations, we~~We use this
165 information to populate the list of offsets in the time series— ~~for the stations’ a priori coordinates~~. In particular, we
166 ~~defined~~define the offsets present in the time series ~~for each station referring to~~ by considering (i) the sitelog information ~~about~~
167 ~~the on~~ station equipment, ~~which allowed defining an offset for each antenna change~~; (ii) the offsets reported by EUREF and
168 IGS, ~~and we excluded only offsets due~~except those related to changes in the processing procedure; (iii) the occurrence of
169 earthquakes with magnitude greater than 5.0 as reported by ANSS catalogue (U.S.G.S., 2017), ~~thus we with an offset~~ assigned
170 ~~offsets~~ to each station insidewithin an empirical radius of influence ~~depending on~~ as a function of the magnitude (using the
171 *sh_makeeqdef* program inside the GAMIT/GLOBK software, Herring et al., 2018).

172 ~~Other~~Another important information reported in the ~~log sheets~~sitelog of a GNSS ~~site~~station concerns the monument type and
173 its location (on a building roof, on a building wall, or on the ground). The monument for a GPS/GNSS site should be designed
174 to provide stable and secure support to mount the antenna. Therefore the monument should comply with a certain number of
175 characteristics. The IGS ~~provides~~and University NAVSTAR Consortium (UNAVCO) provide some recommendations for
176 the ~~monument~~ itselfmonumentation and the ~~monument~~installation site
177 (<https://files.igs.org/pub/station/general/IGS%20Site%20Guidelines%20July%202015.pdf>). ~~The material with which the~~
178 ~~monument is built should guarantee, within a reasonably low cost for building and maintenance, stability with time, corrosion~~
179 ~~resistance, long term survivability, zero interaction with signal, resistance to frost action and temperature variations, with a~~
180 ~~minimum amount of metal in the proximity of the antenna. The site selected for placing the monument should be easily~~
181 ~~accessible, clear of reflecting surfaces that can lead to multipath problems, with a shallow high-quality bedrock, clear horizon,~~
182 ~~with no local instabilities (the presence of faults, karstic cavities, the moisture content in soil rocks, or soil compression,~~
183 ~~should be checked), and with controlled vegetation. The monument site should finally be provided with continuous electric~~
184 ~~power and should guarantee data accessibility remotely (see also~~
185 ~~at~~<https://files.igs.org/pub/station/general/IGS%20Site%20Guidelines%20July%202015.pdf>,
186 <https://kb.unavco.org/article/unavco-resources-permanent-gps-gnss-stations-634.html>). It is not always easy to accomplish
187 all these requirements, because ~~of the difficulties in gathering it is~~ difficult to cover all the conditions and because the same
188 environment changes with over time, especially near urban areas, due to urban developments. The consequences of ~~not~~

189 ~~optimum~~non-optimal site conditions are likely ~~reflect~~to be reflected in ~~the~~ data quality, noisy time series, and increased
190 uncertainties.
191



192



193

194 Fig. 5: Information on the location and monument type of the GNSS stations considered in this study. a) Stations classified
195 according to their location. Rock = ~~site~~station installed on hard terrain (not soil) or outcropping rocks. Building = ~~site~~station
196 installed on a building or similar manufacts, like a wall, both on roof or fixed to the side wall. Soil = ~~site~~station installed on a soft
197 terrain. Unknown = ~~sites~~station whose location description is incomplete or ambiguous. b) Stations not on buildings classified
198 according to monument type. Steel pillar = monument made by a steel column. Steel mast = monument made by a steel bar.
199 Concrete pillar = monument made by a concrete column with or without steel bars inside. Shallow drilled braced = monument
200 consisting of a tripod drilled in the terrain). Miscellaneous includes mixed or not specified material.

201

202 The ~~log sheets~~site~~log~~ of a GNSS site should ~~clearly report the monument's~~provide a detailed description ~~of the monument~~
203 (material type, monument foundation, high and depth of the foundation, geological characteristics of the bedrock, spacing of
204 eventual fractures in the bedrock, presence of faults nearby) ~~with~~accompanied by a ~~photo~~photograph of ~~it~~the same. However,
205 ~~log sheets~~site~~logs~~ are often incomplete and lack images. Figure 5 shows the monument information retrieved from the ~~log~~
206 ~~sheets~~site~~logs~~ of our stations. Hence, we classify as anonymous the monument locations whose description in the ~~log~~
207 ~~sheets~~site~~log~~ is incomplete or ambiguous, and no photos or other sources of information are available to verify the data (Fig.
208 5a).

209 For ~~the~~ stations installed on the roof or the wall of a building, we can ~~reasonably~~ assume that the stability is more affected by
210 the edifice, than by the monument's composition (a steel mast or a concrete pillar). Therefore, we classify ~~according to the~~
211 ~~monument material~~ only the stations located away from buildings ~~according to the monument material~~ (Fig. 5b).

212 As can be noticed from the figure, the majority of stations are located on buildings/walls (251), and just one-third (107) of
213 ~~sites~~stations are located in the free-field (10 on soft soil, 57 on exposed rocks, and 40 are on unknown free-field locations).
214 Approximately 50% of the latter have concrete pillars as monuments (54), ~10% have a monument composed of steel rods
215 or a steel tripod (shallow drilled braced, http://ring.gm.ingv.it/?page_id=43) (11), while ~~the rest~~ of the ~~rest, 9~~stations have
216 steel mast monuments, ~~6 have (9)~~, steel pillar equipped stations ~~and 27 have (6) or~~ not defined monument types: ~~(27)~~.

217 3 Data processing

218 We process the ~~GNSS~~GPS data using the GAMIT/GLOBK software package (ver 10.71) (Herring et al., 2018). GAMIT can
219 estimate station positions, atmospheric delays, satellite orbits, and Earth Orientation Parameters (EOP) from ionosphere-free
220 linear combination ~~of~~ GNSS phase observables, ~~by~~ using ~~the~~ double-differencing ~~technique~~technique to eliminate phase
221 biases caused by drifts in the satellite and receiver clock oscillators. It outputs loosely constrained solutions (h-files) of ~~the~~
222 parameter estimates and their covariance matrix. GLOBK is a module ~~that~~which implements ~~the~~ Kalman filtering, and it is
223 used to combine ~~the~~ loosely constrained solutions (between networks and through time) and ~~to~~ constrain the results into a
224 consistent reference frame.

225 We process ~~GPS~~the data following these steps:

- 226 ● definition of ~~the~~ sub-networks (subsets of stations);
- 227 ● computation of ~~the~~ loosely constrain solutions for each sub-network;

- combination of the sub-networks solutions and computation of the daily position for each station;
- computation of the GNSS station velocities.

The RINEX files available each day are processed after being divided into subnetworks to pursue computational efficiency. To do that, we use the *netset* program of the GAMIT/GLOBK software package, which considers the geographic distribution of the stations in order to build the subnetworks (see Serpelloni et al., 2022 for a detailed description of the algorithm). Each subnetwork is linked to the next one by one station. An additional sub-network that contains two tie sites from each sub-network links all the sub-networks together. We perform some tests to identify the best nominal number of stations for each subnetwork, which depends on the ~~total amount of~~ data available: we select 30 stations/subnetwork until 2008 and 40 stations/subnetwork for the following years. ~~The data~~ Stations from SLO_GPS network are equipped with ~~old~~ receivers, ~~which whose data~~ need to be elaborated using the LC_HELP algorithm of the GAMIT/GLOBK software, which uses ~~an~~ ionospheric ~~constraint~~ constraints. To include these stations in the solution, we process them ~~and in a separate sub-network~~ along with some tie sites (TRIE, GSR1 and KDA2) ~~in a separate sub-network.~~. The tie sites of this sub-network will be excluded from *netset* site list and ~~then~~ added to the tie sites sub-network afterwards. We compute the loosely constrained solutions using the GAMIT module. GPS phase data are weighted according to an elevation-angle-dependent error model (Herring et al., 2018) using an iterative analysis procedure whereby the elevation dependence is determined by the observed scatter of phase residuals. ~~The parameters of satellite orbit are fixed to the IGS final values.~~ Satellite precise orbits are retrieved from IGS repository (<http://www.igs.org/products/>, Johnston et al., 2017). The first-order ionospheric delay is eliminated by using the ionosphere-free linear combination for all the stations except the SLO_GPS ones. Further details about models and parameters are reported in Table 1.

Table 1: GAMIT solution parameters.

Parameter	
Processing mode	Baseline - orbits parameters are not estimated
Elevation cutoff	10°
<u>Precise orbits</u>	<u>IGS final products in SP3 format</u> <u>(https://www.igs.org/products/#orbits_clocks)</u>
<u>Broadcast Ephemeris data</u>	<u>RINEX navigation files from the Scripps Orbit and Permanent Array Center (SOPAC, http://sopac-csrc.ucsd.edu/) or from the Crustal</u>

	Dynamics Data Information (http://cddis.nasa.gov, Noll, 2010)
Magnetic field	IGRF13 (Alken et al., 2021)
Ionospheric model	2nd-order ionospheric products ionosphere corrected through IGS IONEX files
Earth Orientation Parameters (pole position and UT1 and their rates of change)	Tightly constrained to <i>a priori</i> values obtained from IERS Bulletin A
Earth Rotation Model	IERS 2010 (Petit and Luzum, 2010)
Solid Earth tides	IERS 2010 (Petit and Luzum, 2010)
Ocean tidal loading	FES2004 (Lyard et al., 2006)
Atmospheric non tidal loading	Not applied
Atmospheric tidal loading	Not applied
<i>A priori</i> atmospheric parameters (pressure, temperature, zenith delay)	VMF1 VMF1 grid (Vienna Mapping Function 1, Boehm et al., 2006)
Zenith delay estimation	estimates at 2-hr intervals for a 24hr session using a piecewise-linear (PWL) function
Tropospheric mapping function	VMF1 VMF1 grid (Vienna Mapping Function 1, Boehm et al., 2006)

252

253

254

255

256

257

258

259

260

261

262

263

~~The~~ To obtain the position time series, we use the GLOBK module to combine the daily loosely constrained solutions of the subnetworks ~~are combined and expressed in a single daily solution leaving the constraints free. Since we want to express the~~ solutions in the International Terrestrial Reference ~~frame~~ Frame (ITRF14/IGS14 by Altamimi et al., 2016; in particular, we use the newer GNSS geodetic reference frame IGB14) ~~to obtain the position time series of each station. We), we then apply~~ generalised constraints (Dong et al., 1998) using the glorg program. For this purpose, we use a six-parameter Helmert transformation (translation and rotation) estimated by minimising the difference ~~of~~ in the positions of a set of stations with well-defined coordinates and velocities (reference sites) as ~~to~~ a priori coordinates. ~~We must keep both the coordinates and the EOP loosely constrained. We do not explicitly use scale to do that. By visual inspection of the~~ avoid potential absorption of height signals, following Herring et al. (2016). The results are daily position estimates for each station consistent with the IGB14 reference frame.

264 ~~The time series, we are visually inspected to~~ identify offsets that are ~~unrelated~~~~not due~~ to ~~changes in the~~ equipment ~~changes~~
265 or ~~to~~ earthquakes. We ~~automatically~~ remove outliers ~~automatically~~ using two criteria similar to those ~~of~~~~used by~~ Floyd et al.
266 (2010). First, we remove ~~the~~ daily positions that have formal uncertainty greater than 20 mm. Then ~~we fit~~ the time series ~~were~~
267 ~~fitted to a model by a weighted linear regression~~ to a model consisting of a linear trend and offsets ~~through a weighted linear~~
268 ~~regression~~ by using the *tsfit* program. ~~Positions~~~~The positions~~ with residuals greater than three times the weighted root-mean-
269 square (RMS) value of the fit ~~were~~~~are~~ also removed. Finally, ~~from the analysis of the time series cleaned from the outliers,~~
270 ~~we estimated the random walk values for each site, and we identified some sites to remove because of the noise level (random~~
271 ~~walk value greater than 2.0 mm²/yr), by~~ applying the *real_sigma* algorithm (Floyd and ~~Harring~~~~Herring~~, 2019), which allows
272 ~~taking into account~~~~accounting for~~ temporal correlations in the data, ~~we estimate random walk values for each station from~~
273 ~~the analysis of the outlier-adjusted time series and identify specific sites exhibiting a random walk noise level exceeding 2.0~~
274 ~~mm²/yr level, which are also removed.~~

275 ~~We~~

276 ~~To~~ compute the ~~velocity~~ field, we use the forward-running Kalman filter implemented in the GLOBK module, in which the
277 ~~state vector includes the positions and~~ velocities ~~and coordinates of for~~ each station ~~by combining all the cleaned~~ (~~Herring et~~
278 ~~al., 2016~~). ~~The input data are the~~ daily ~~loosely constrained~~ solutions. ~~In order to express the solution in other reference frames~~
279 ~~(e.g., ETRF14, Altamimi et al. 2017), we,~~ as they may be freely rotated and translated, thus ~~eliminating the~~ need to ~~estimate~~
280 ~~rotations and rotation rates independently~~~~include~~ EOP in the state vector, and their full variance-covariance matrices.
281 ~~Following~~ Herring et al. (2016), from the analysis of the previously generated time series, we retrieve the list of EOP ~~since~~
282 ~~they are not included in the GAMIT solutions. Intending~~ outliers to be excluded from the computation and the site specific
283 ~~parameters to~~ ~~reduce the computational time, we again~~ model the stochastic noise on the station positions. At each epoch, the
284 ~~Kalman filter updates positions and velocities. With the aim of reducing the computation time, we~~ divide the stations into
285 sub-networks using *netset*. We use a nominal number of 90 ~~sites~~~~stations~~ for each sub-network and the noise model obtained
286 from the time series analysis. First, we estimated the velocities and positions of the ~~stations~~ included ~~stations for~~ in each sub-
287 network. ~~Hence~~~~Then~~, we combine the solutions obtained for each sub-network in a ~~unique~~~~single~~ solution ~~expressed in~~. ~~At~~
288 ~~the end of the forward Kalman filter run, we align positions and velocities to the~~ IGB14. ~~Then,~~ reference frame using twelve
289 ~~parameters~~ Helmert transformation (rotation, translation and their rates). Velocities of stations within 1 km distance (including
290 ~~differently named stations at the same location) are equated~~ in a ~~second step, we recompute~~ this reference frame realisation.
291 ~~Finally, we recalculate~~ the time series and velocities using, ~~as a priori coordinates, the resulting the~~ values obtained in the
292 previous iteration ~~while extending~~~~as a priori coordinates and expand~~ the list of ~~stabilisation sites~~~~reference stations~~ to include
293 all ~~sites~~~~the stations~~ with random walk values lower than 0.5 mm²/yr. ~~Finally, we~~ As reported by Herring et al. (2018), the
294 ~~time series that best represent the final velocity solution are those computed considering all stations in the solution as reference~~
295 ~~sites. We also~~ express our solutions relative to the Eurasia plate as defined by Altamimi et al. (2017) plate motion model
296 ~~(ETRF2014). ETRF14 reference frame) using the same procedure adopted for IGB14.~~

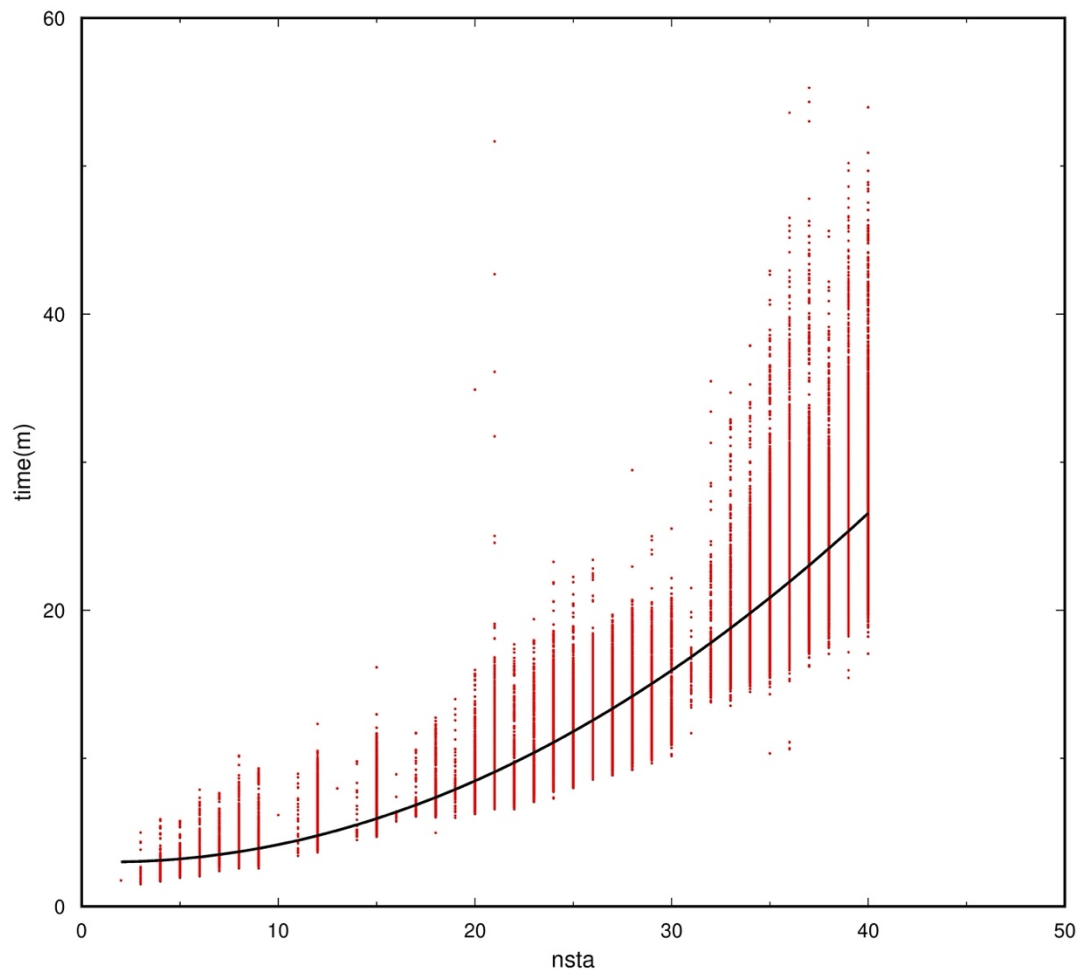
297

298 3.1 Computing infrastructure

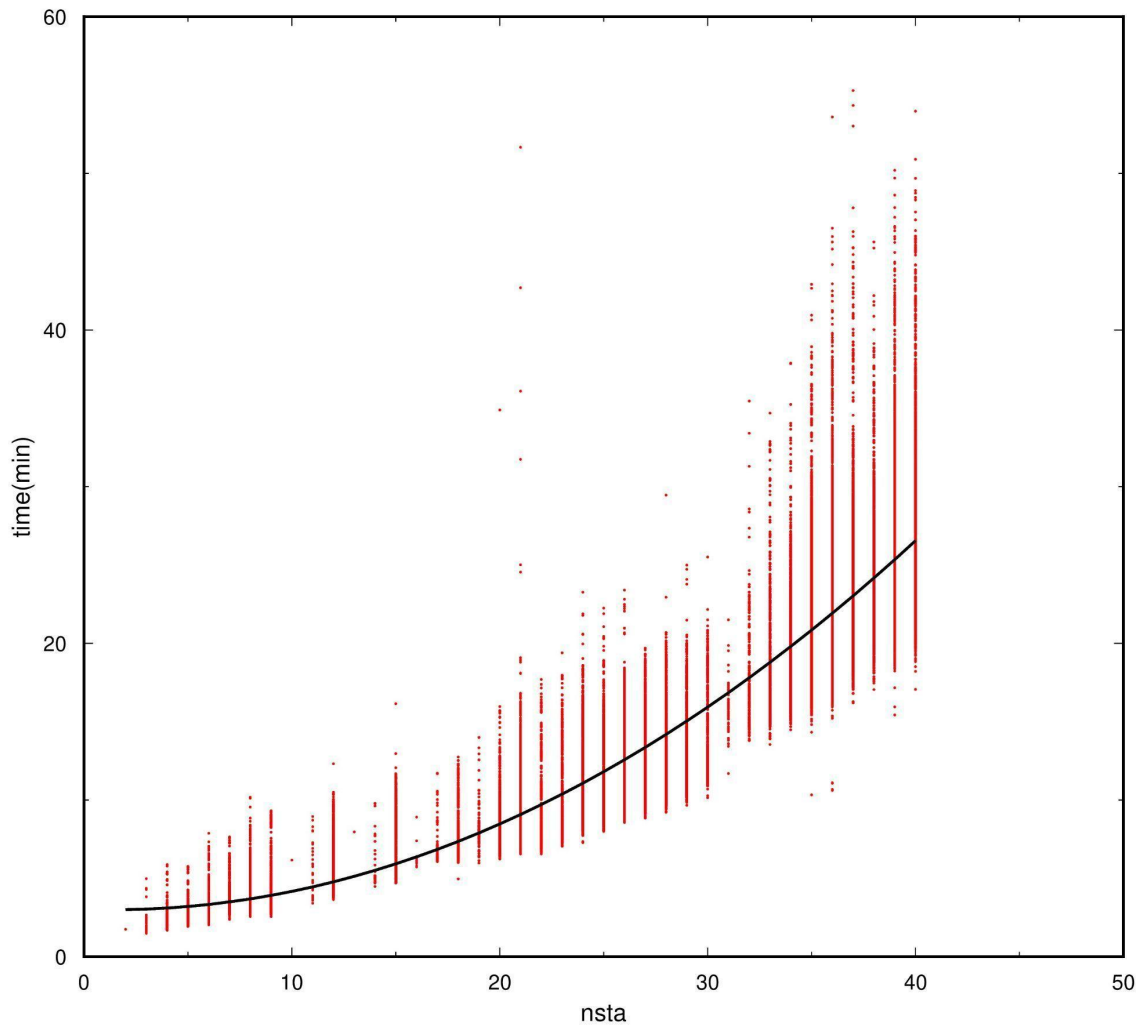
299 Modern computational infrastructures allow the analysis of huge amounts of data with extraordinary advantages in terms of
300 operational cost for data storage, processing and time-saving, leading to the timely provision of homogeneous products. We
301 exploited the CINECA (<https://www.hpc.cineca.it/>) High-Performance Computing (HPC) resources to process and analyse
302 in a very short time all the GNSS data available in the study area between 2002, January 1st and 2022, June 30th. We used
303 the GALILEO100 Cluster, which is equipped with 554 compute nodes with 2 x CPU Intel CascadeLake 8260 each with 24
304 cores, 2.4 GHz, 384GB RAM DDR4. The job scheduling and workload management system is SLURM 21.08
305 (<https://wiki.fysik.dtu.dk/niflheim/SLURM>). SLURM is designed to accomplish three key functions: (i) allocation of
306 exclusive/non-exclusive access to computing nodes to users for a specific duration of time; (ii) provision of a framework for
307 managing the work (starting, execution, monitoring) on the set of allocated nodes; (iii) resources distribution handling by
308 managing a queue of pending jobs.

309 Figure 6 ~~aims~~ ~~intended~~ ~~to~~ ~~hint~~ ~~at~~ ~~give~~ ~~an~~ ~~indication~~ ~~of~~ the performance of CINECA clusters for GNSS data elaborations ~~by~~
310 ~~reporting~~ ~~showing~~ the ~~calculation~~ ~~computation~~ time on GALILEO100 ~~compute~~ ~~computing~~ nodes to obtain the GAMIT
311 solutions ~~in~~ ~~the~~ ~~as~~ ~~a~~ function of the number of ~~sites~~ ~~stations~~ considered on each job sent to ~~the~~ compute nodes. The figure
312 shows that the ~~calculation~~ ~~computation~~ time varies on average with the square of the number of ~~sites~~ ~~stations~~. Although the
313 calculations of the GAMIT solutions are the most time-consuming jobs of the processing procedure, the total computation
314 time on GALILEO100 depends not only on the number of available daily data but also on the adopted parallelization strategy
315 (i.e., the number of jobs sent to resources on compute nodes) and the occupancy of the machine (i.e., ~~the~~ queue waiting time).
316 In our study, we managed to process two decades of GNSS data in one week. We implemented the same procedure described
317 in the previous section on a local machine to process the data daily following the 30th of June 2022, with the aim of keeping
318 the products updated. The daily processing is automated by using the crontab utility. More details on the implementation on
319 the local machine can be found in the Appendix B.

320



321



322

323

Fig. 6: Calculation time for GAMIT solutions using GALILEO100 cluster in function of the number of sites (nsta).

324

4 Geodetic time series and velocities dataset

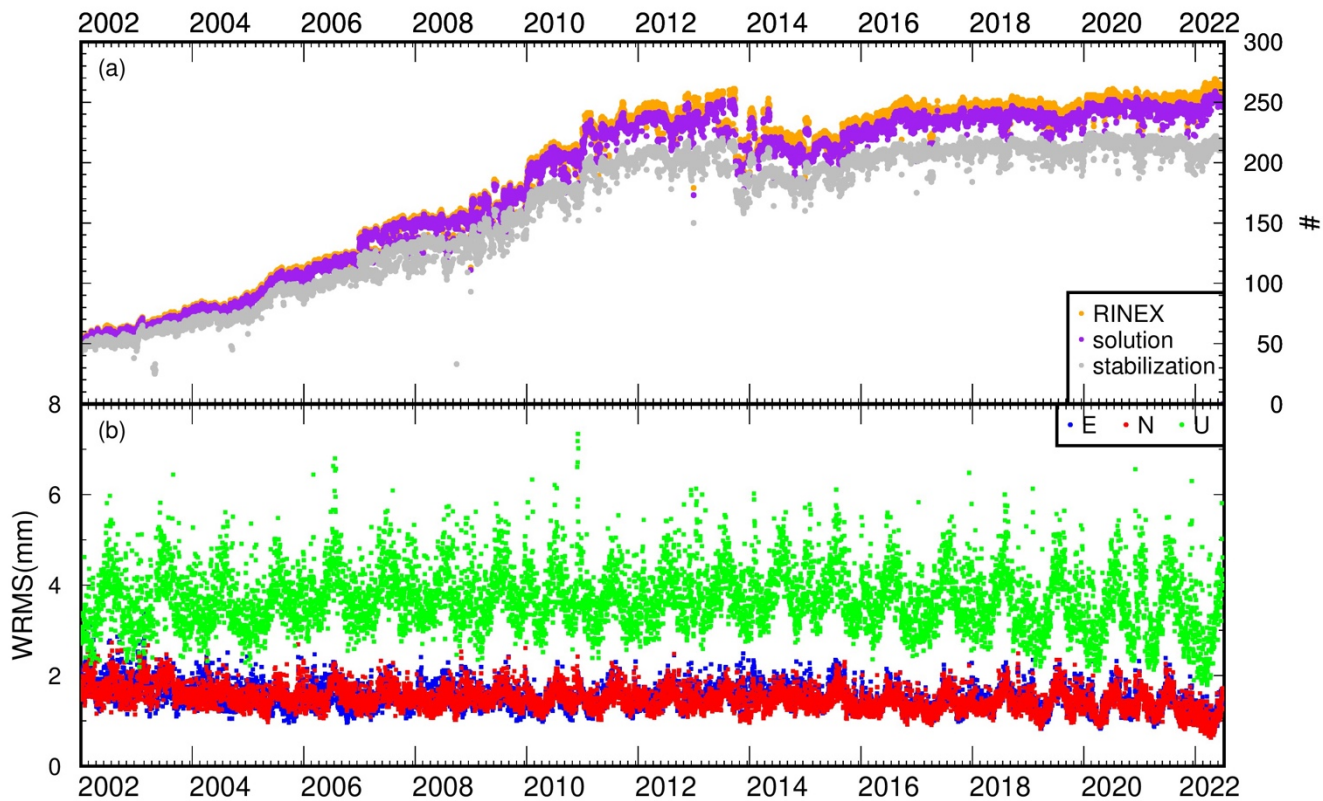
325

This section ~~presents~~considers the geodetic time series and velocity products provided. In support of the dataset, we illustrate several tests performed to check the reliability of the documented results. For the sake of simplicity, we define the results of this study as “final time series” and “final velocities”, and those estimations retrieved from the tests as “test time series” or “test velocities” .

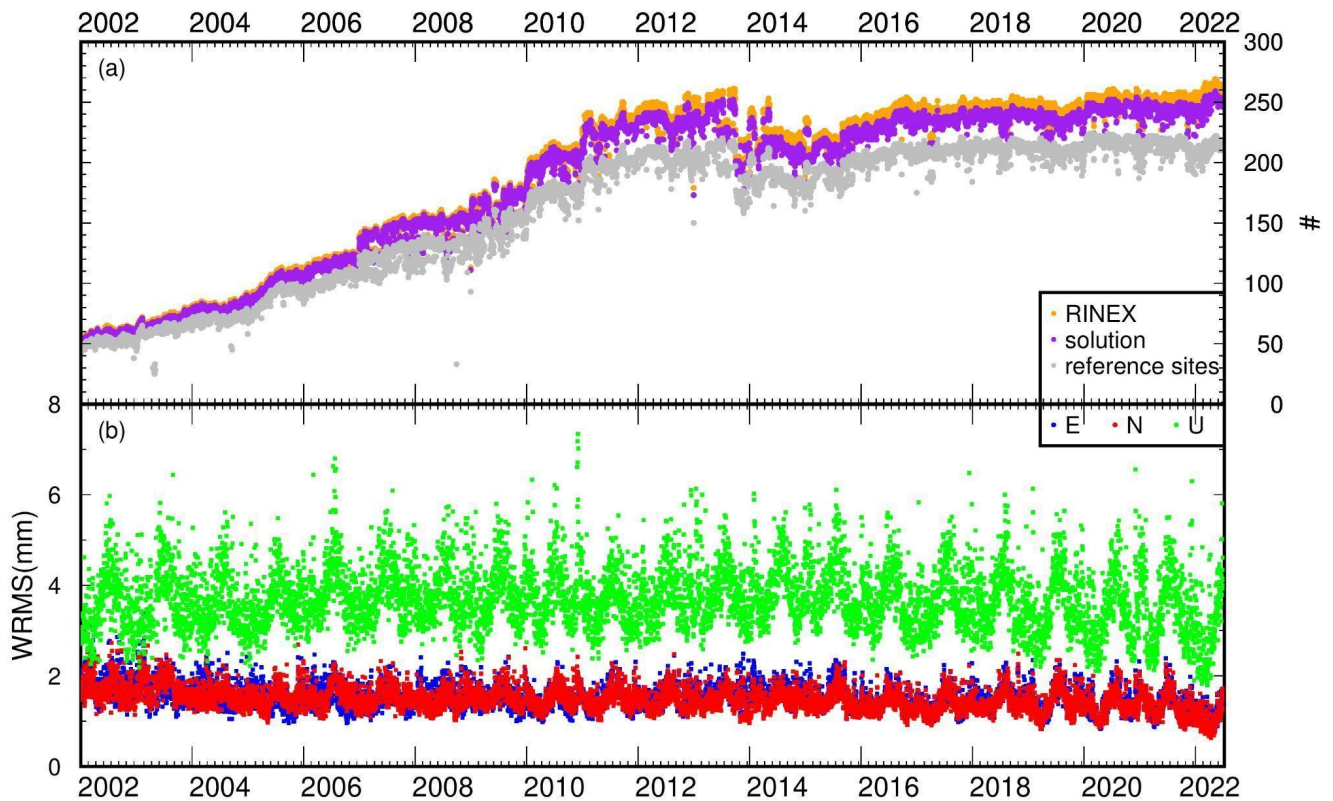
328

329 **4.1 Time series quality**

330 We illustrate here the GNSS time series resulting from the data processing as a whole, whereas time series for single stations
331 are provided in the dataset, as explained above.



332



333

334 **Fig. 7: (a) Evolution of RINEX data available with time (orange dots), sitesstations included in the solutions (purple dots) and**
 335 **sitesstations being used in the reference frame realisation (grey dots); (b) weighted root-mean-square (WRMS) scatter of the fits**
 336 **to the coordinates of the reference frame stations in North (red), East (blue) and Up (green) components.**

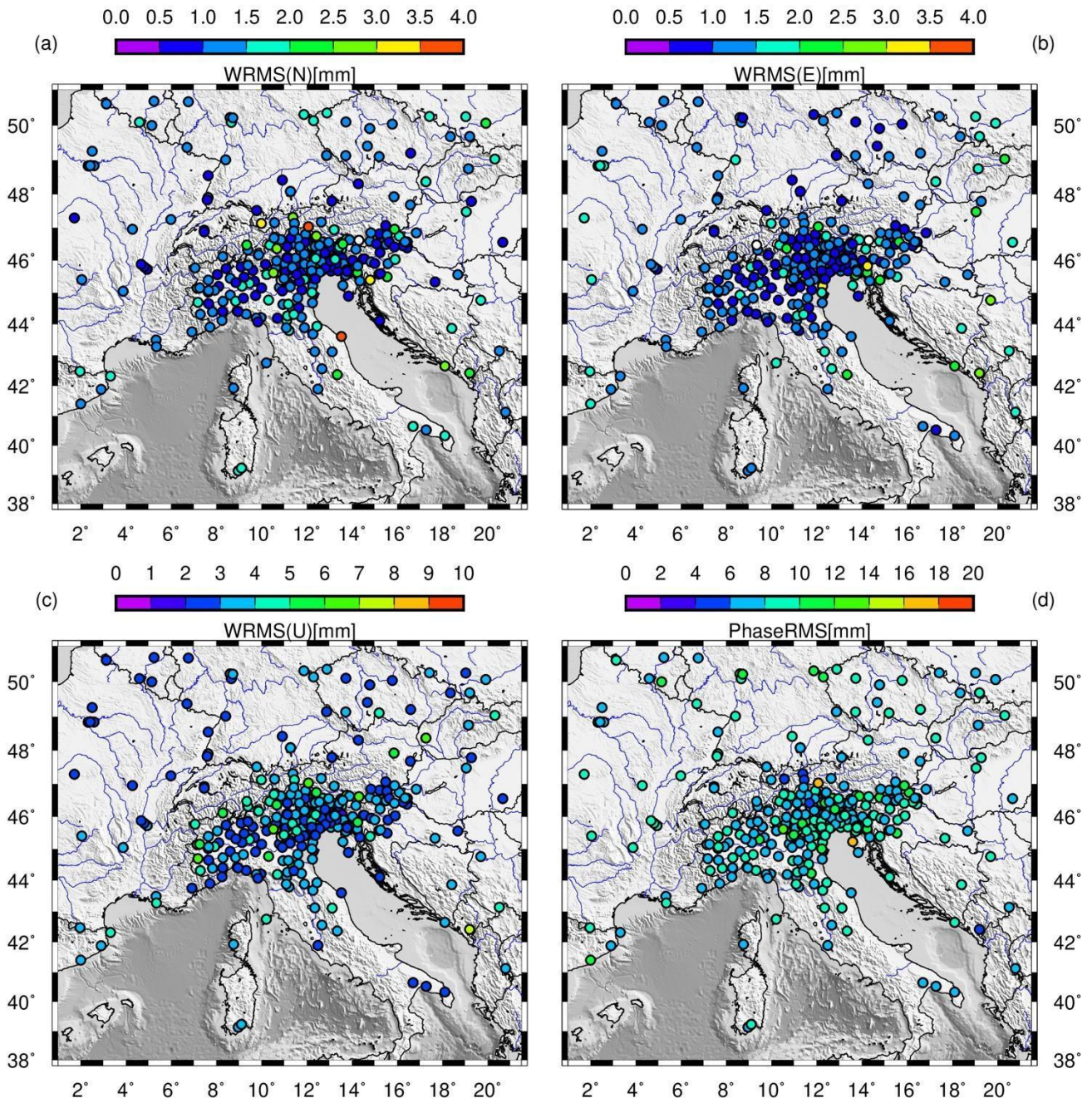
337

338 The time-series length and quality depend on the number of good observations recorded at the sites, which is reflected in the
 339 number of solutions obtained for each station. Figure 7 shows the evolution of RINEX available with time, the sites included
 340 in the solution, and those being used in the reference frame realisation, along with the weighted-root-mean-square (WRMS)
 341 of the fits to reference frame stations. Through data processing, the recorded RINEX allowed obtaining almost 97,1% of
 342 solutions (purple dots in Fig 7a), a percentage which is indicative of the goodness of the dataset and of the adoption of an
 343 appropriate processing strategy. The percentage of missing solutions (~3%) is mainlyare likely due to incomplete data records
 344 (RINEX with less than 864 daily observations, i.e., with less than 30% of registrable daily observations) or stabilisation
 345 errors-bad data. As illustrated in Section 3, in order to stabilise the solution we consider all sitesstations with a random walk
 346 value lower than $0.5 \text{ mm}^2/\text{yr}$, which led to consider as stabilisation sites—reference stations ~80% of the available sitesstations
 347 after 2011, and even ~90 % or more in the first decade (grey dots in Fig. 7a). The average WRMS fit to the reference frame

348 stations (Fig. 7b) is 1.7, 1.8, and 4.2 mm in North, East, and Up components, improving up to 20% in the latter since 2011,
349 possibly thanks to the equipment improvements.

350 Figure 8 shows the stations' noise level through the representation of the WRMS of the time series and the RMS of the phase
351 residuals. Notably, the 90% of the stations show low noise levels, with values below 2 mm in the horizontal components and
352 below 4.1 mm in the vertical one.

353



354

355 **Fig. 8: Time series WRMS in the horizontal (a, b) and vertical components (c) and time series RMS of the phase residuals (d).**

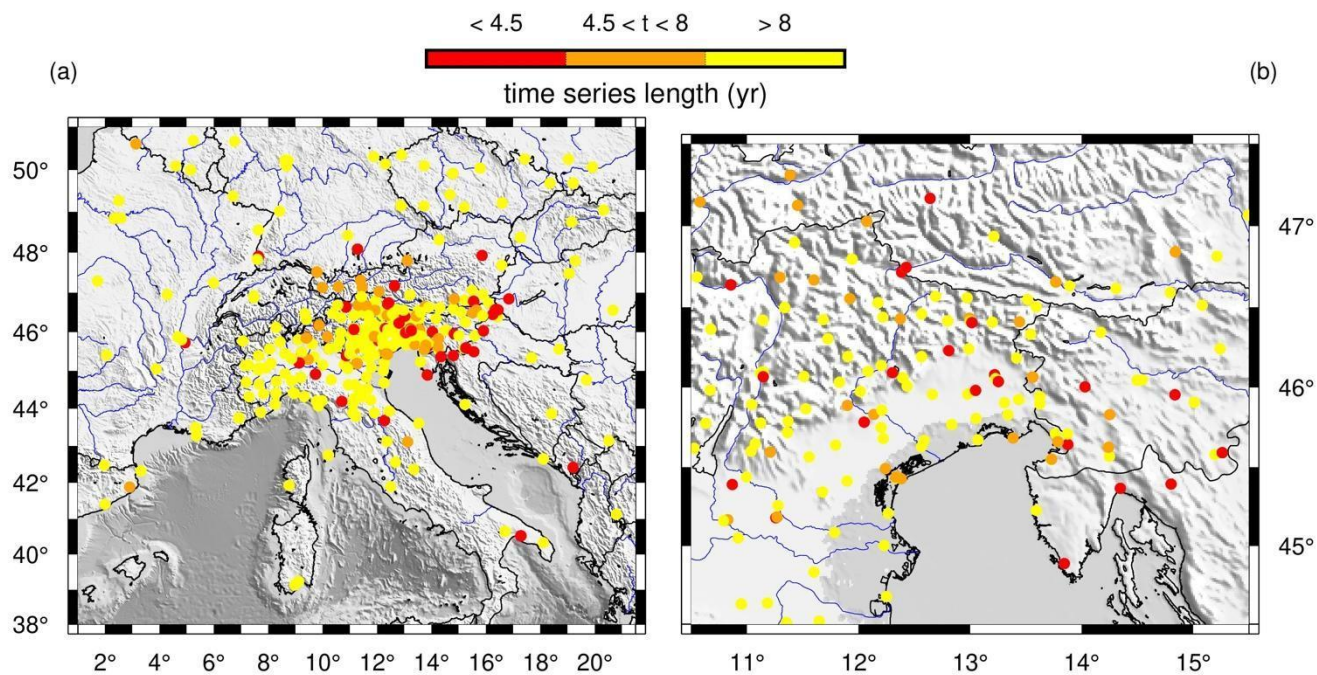
356

357 4.2 Geodetic velocities

358 ~~Time-series~~The length ~~is widely recognized as of the time series is generally considered~~ fundamental ~~for defining in~~
359 ~~determining~~ the accuracy and precision of the estimated linear velocities. ~~For example,~~ Blewitt and Lavallee (2002) show that
360 ~~2.5 years of a~~ coordinate time series ~~of 2.5 years~~ is the minimum ~~span~~range to reduce velocity errors due to annual time series
361 signals, ~~caused~~ primarily ~~caused~~ by surface loading due to hydrology and atmospheric pressure. However, the ~~use of data~~
362 ~~spans greater~~authors recommend using time series longer than 4.5 years ~~is preferable to almost completely~~ eliminate velocity
363 ~~bias almost totally.~~ Masson et al. (2019) agree with this study, affirming that data spanning ~~biases.~~ Data over a period less
364 than 4.5 years are not suitable for studies ~~that require precision lower~~requiring an accuracy of less than 1 mm/yr and ~~that~~ the
365 best ~~would be achieved~~results are obtained by using long time-series (>8 years ~~in length~~) which allow ~~the estimation of~~
366 velocities ~~to be estimated~~ with an accuracy of 0.2 mm/yr ~~accuracy~~ in the horizontal components and 0.5 mm/year ~~on~~in the
367 vertical component. (Masson et al., 2019).

368

369



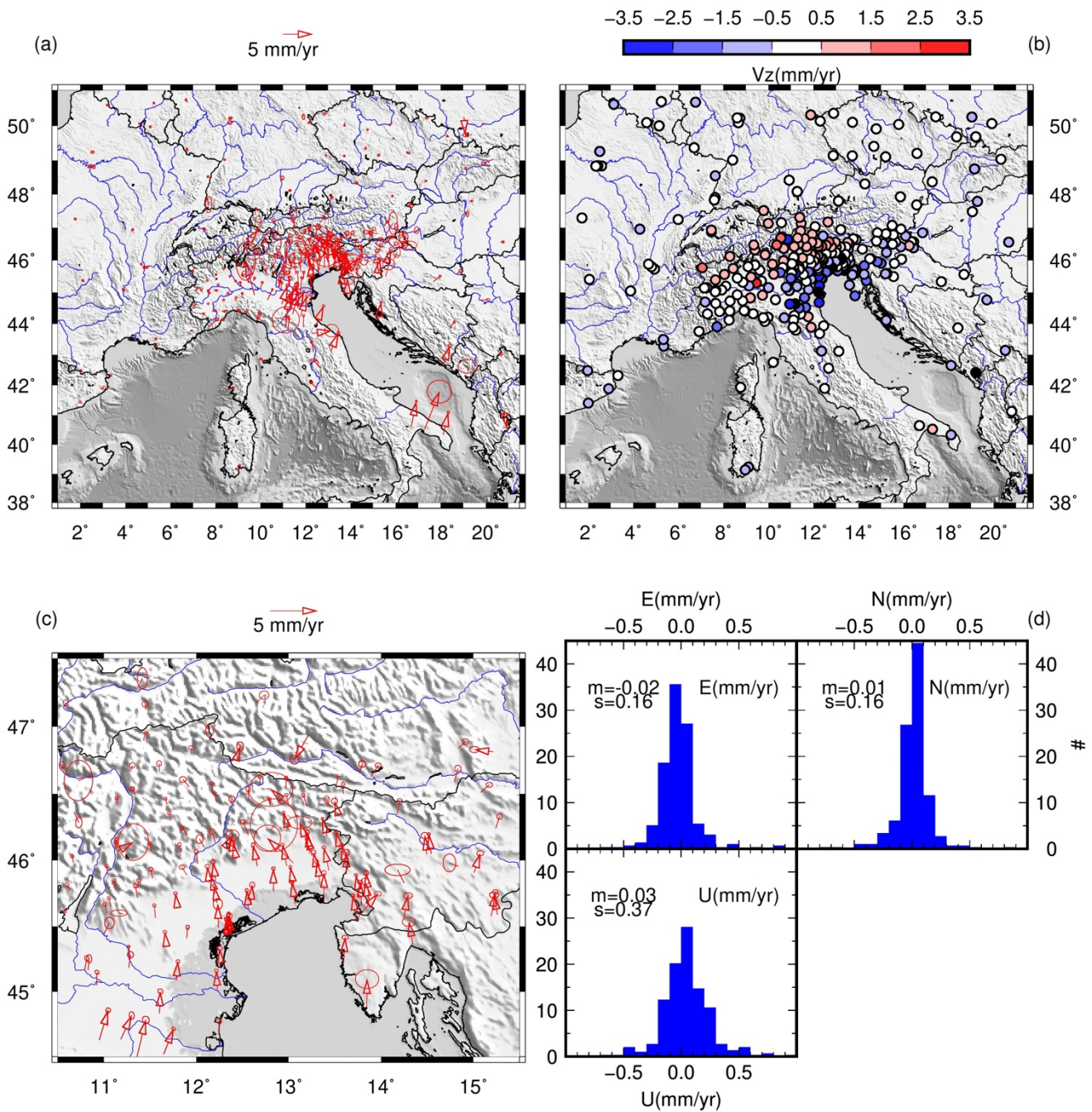
370

371 Fig. 9: Time series length of the stations considered in this study: (a) with a zoom in the NE-Italy (b).

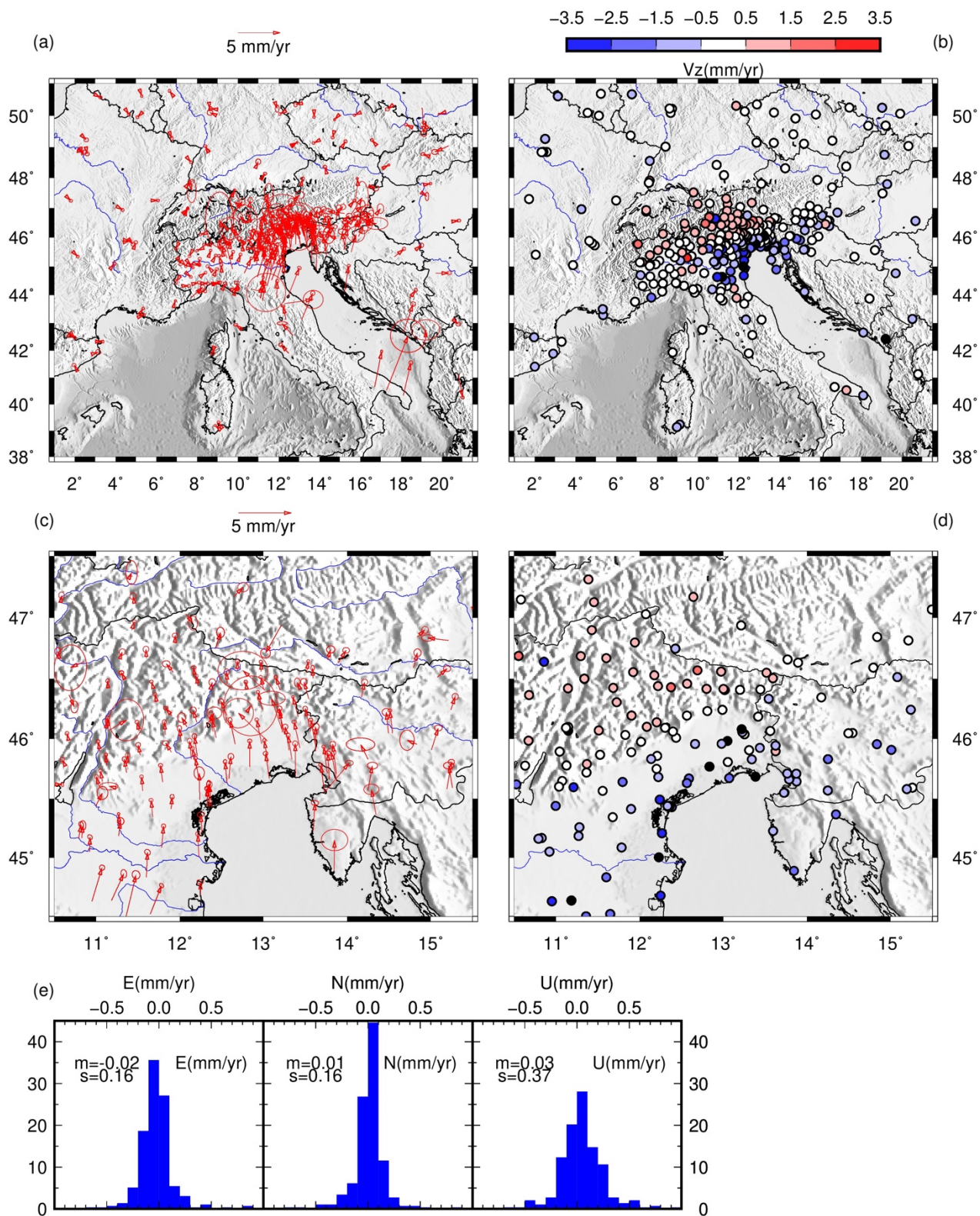
372

373 The stations considered in our study provide time series spanning from 0.27 (HELM) years to 20.49 years (~~between~~among
374 others, we cite AQUI, GENO, GRAZ, GSR1, and TORI), as shown in Fig. 9. Most of the sites provide time series longer
375 than 4.5 years (84.4%), and even longer than 8 years length (69.4%), whereas just a small percentage are ~~young~~new stations
376 providing coordinate time series shorter than one year (8.9%). However, ~~younger~~newer stations are often located in proximity
377 to older stations, thus allowing the retrieval of reliable and stable results also for that particular area (see Fig. 9b).

378



379
380



382 Fig. 10: Estimated velocities with 95% confidence error ellipses, in the horizontal (a, c) and vertical components (vz) (b, d). (e)
383 Histograms indicating the differences, along the three components, between velocity estimates calculated with GLOBK using the
384 procedure described in Data Processing section, and those calculated using *tsfit* considering the stations with minimum 4.5 years
385 long time series. Overall the differences are in a Gaussian shape, with mean and standard deviations values firmly below the mm/yr.

386
387 We estimated the velocities and uncertainties of all stations for the horizontal (Fig. 10a,c) and vertical components (Fig.
388 10b,d) using the GLOBK software. For completeness, we have also calculated the velocities using *tsfit*, a program
389 ~~allowingthat provides~~ a linear fit of the time series, and we have compared the results (Fig. 10e) finding sub-millimetre
390 ~~ordermillimeter~~ differences. The estimated velocities in ETRF14 show the active deformation in the Adriatic side of the
391 Central Apennines, in the few stations located in the SE-Italy (Puglia region) and in the NE-Italy, with horizontal displacement
392 directed to the North-East with values of 2-3 mm/yr in the Apennines and also in the Friulian plain and coast. The NE-Italian
393 Alps, instead, move with slower rates rounding 1 mm/yr. Significant horizontal motion is estimated in the SE-Italy, especially
394 in the North velocity component, with 3.8 mm/yr and 4.2 mm/yr at USAL and MATE stations, respectively. The fastest
395 motion (~ 7 mm/yr) is estimated at TARS and FATA stations (located close to each other and indistinguishable at the scale
396 of Fig. 10). However, this value is not reliable because these stations provide less than 1-year of observations, as it can be
397 inferred from the high uncertainty. The estimated vertical displacement highlights the subsidence in the Po Basin (up to 3.5
398 mm/yr) and the uplift in the mountains, more accentuated in the Eastern Alps than in the Apennines. Beside the European
399 reference ~~stationsites~~ located beyond Italian territory, also the stations in the NW-Italy show no significant displacement.
400 The single exception is LODI station, whose anomalous behaviour (~2 mm/yr velocity in the horizontal components and ~
401 2.8 mm/yr of uplift) is due to its location on the top of a depleted methane reservoir, recently converted into an underground
402 gas storage facility (Priolo et al., under review). Zooming in the NE of the study area (Fig. 10c), a pattern of South-North
403 decreasing velocities is distinguishable from the Friulian coastline and plain, to the Southern sector of the Eastern Alps, with
404 an NNW orientation, whereas the stations located in Slovenia and Croatia show NNE oriented velocities. An anomalous
405 south-directed motion is estimated in the OCHS station, in the Eastern Alps, likely due to a landslide motion occurring along
406 the slope where the GNSS station is located.

407 5 Evaluation of the quality and robustness of the dataset

408 ~~Aiming to~~To evaluate the quality and robustness of the dataset, we perform some experiments ~~onwith~~ the processing
409 procedure, ~~analyseanalysed~~ the ~~stations'~~ quality of the stations, and ~~comparecompared~~ our ~~resultsfindings~~ with previous
410 studies.

411 5.1 Data processing tests

412 ~~OnceAfter determining~~ time series, velocities and positions for each station ~~were determined~~, we ~~testedtest~~ their stability and
413 the reliability of the adopted processing ~~adopted~~ procedure. For that, we ~~performedperform~~ a number of experiments on the

414 available dataset to check for potential effects of selected options of the data processing with GAMIT/GLOBK (i.e.,
415 considering or avoiding tidal or non-tidal loadings or changing the ~~stabilisation~~reference stations) on the results. In this way,
416 if these tests do not highlight significant differences with the study results illustrated in the above sections, we can reasonably
417 conclude that our results are reliable and not ~~biased~~biased by processing errors.

418 In one test, we ~~changed~~change the model used to estimate the atmospheric delay. Instead of using the default Vienna Mapping
419 Function numerical weather model (VMF1) calculated by TU Vienna by interpolating hydrostatic and wet mapping function
420 coefficients as a function of time and location (Boehm et al., 2006a), we adopt the Global Mapping Function (GMF) model
421 developed by Boehm et al. (2006b) which fits the European Centre for Medium-Range Weather Forecasts (ECMWF) data
422 over 20 years. Then, since tides and non-tidal loadings are primary sources for time-variable displacements in station
423 coordinates, we perform a test in which we consider the non-tidal atmospheric loading in the processing using a global gridded
424 dataset provided by MIT ~~and a further test, where we remove the ocean tidal loading that was inserted in the procedure~~
425 ~~described in Section 3.~~ For ~~all these three~~both tests, we ~~recalculated~~recalculate the time series ~~for each station~~ and
426 ~~compared~~compare them to the ~~final ones~~original solution, finding no significant dissimilarity, ~~just slight~~with differences
427 ~~inferior to~~below 1 mm~~—, in agreement with previous studies (Steigenberger et al., 2009; Labib et al., 2019)~~

428 Regarding the ~~position time series and~~ velocity estimations, we recall here that one delicate step in the ~~velocity estimation~~
429 procedure is knowing how to ~~edit~~perform editing and ~~weigh~~weighting of the data, ~~define, and realise~~as well as the realisation
430 ~~of the reference frame.~~ To ~~do that~~test these issues, we need to consider ~~what~~which stations to include explicitly, how to treat
431 the orbits and ~~the~~ EOP, and practical constraints on computation speed and data storage. Although the GPS satellites provide
432 a natural dynamic frame for ground-based geodesy, the doubly-differenced phase observations do not tie a ground station to
433 the orbital constellation at the millimetre level ~~we require for scientific studies. Instead, we.~~ We define and realise a precise
434 terrestrial ~~reference~~ frame by applying constraints to one or more sites in our network. To do that, we use the “generalised
435 constraint” method of *glorg*, in which up to ~~seven Helmut~~fourteen ~~Helmert~~ parameters (3 translations, 3 rotations, and 1 scale,
436 ~~and their rates~~) are estimated such that adjustments to *a priori* values of the coordinates of a group of stations are minimised.

437 For continental-scale networks like the one considered in this study, we estimate translation and rotation and include as
438 ~~stabilisation~~reference sites a set of distributed stations for which we have good *a priori* values and sound data.

439 ~~We~~Hence, we perform some tests to check the goodness of the stabilisation frame considered. ~~First~~We ~~recompute~~recalculate
440 ~~the time series imposing by applying the translation-only transformation as for in the EUREF standards (~~
441 ~~<https://www.epncb.oma.be/products-services/analysiscentres/combsolframe.php>), finding and find negligible differences in~~
442 ~~the time series. Then, we~~We then perform ~~conduct~~two ~~some~~ tests ~~on for~~ the first step of velocity estimation, ~~using.~~ ~~Firstly,~~
443 ~~we use~~ as ~~stabilisation~~reference sites two different subsets of the reference sites set used in the final processing (see Test-1
444 and Test-2 in Fig. C1 in Appendix C). ~~Secondly,~~ on the second step of velocity estimation, we consider a regular grid of
445 reference sites ~~as stabilisation sites~~, generated considering a site every 2° (~ 222 km) (see Test-3 in Fig. C1 in Appendix C).
446 Finally, we calculate the velocity field in our study area for each test. Overall, the mean difference values with respect to final

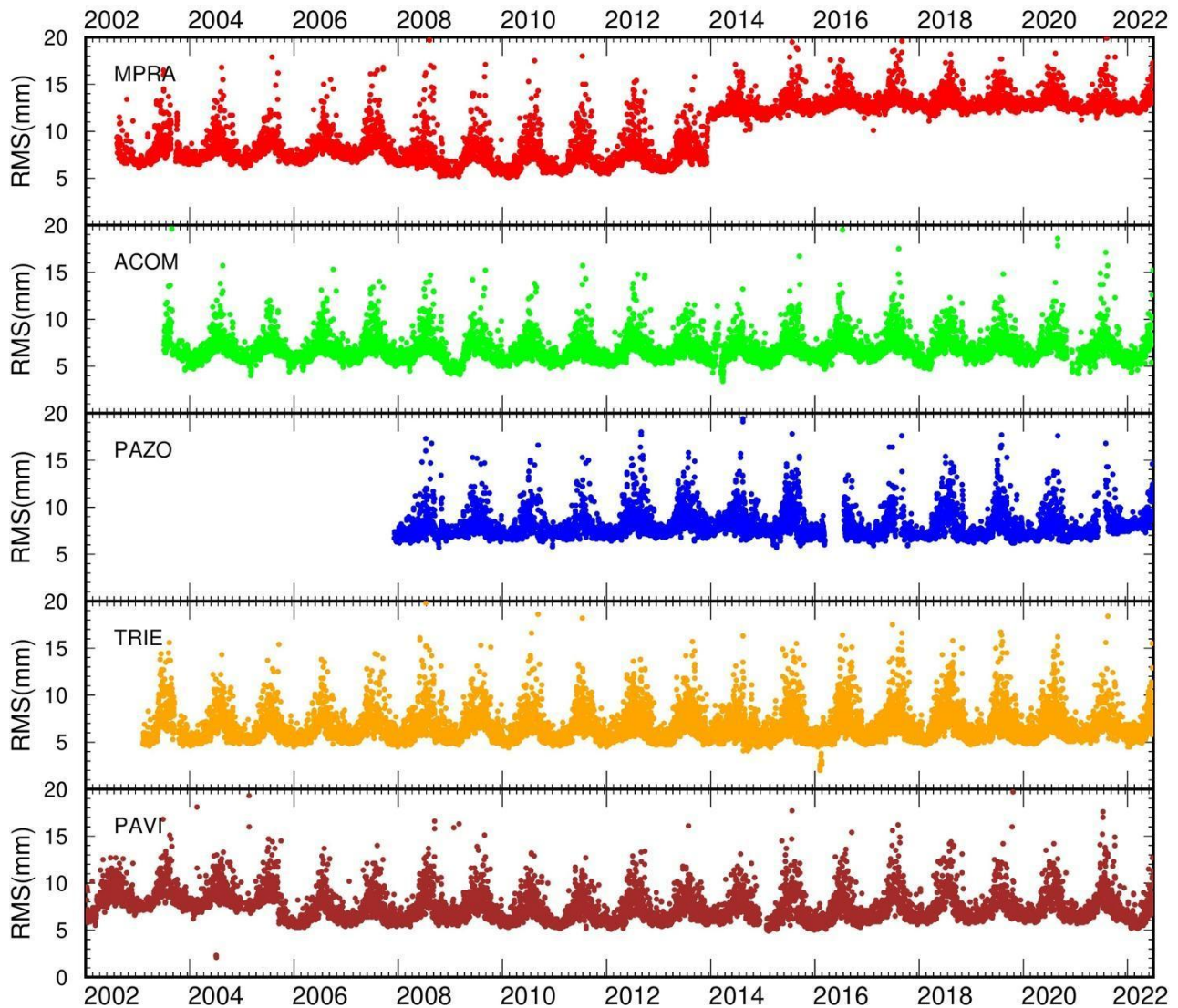
447 velocities are very ~~low~~small, ~~which i.e. means~~ up to 0.02 mm/yr in the North, up to 0.06 mm/yr in the East and Up to 0.14
448 mm/yr in the vertical component.

449 Finally, we perform two last experiments to evaluate the effects on the velocity results of introducing the periodic term (annual
450 signal) in the coordinate time series fitting and applying a less restrictive criterion for outliers, i.e., 5 sigmas instead of 3
451 sigmas. The mean differences, with respect to the final velocities, are of the order of 0.02 - 0.03 mm/yr in both cases for
452 stations with at least 4.5 years of time series length.

453 **5.2 Considerations on the stations quality**

454 The ~~time changes in the environmental~~alteration of the ~~surroundings of~~environmental conditions surrounding a GNSS station
455 ~~affect~~affects the RMS of the phase residuals. The ~~environmental~~ changes can be related not only to climatic conditions, ~~with~~e.
456 ~~g.~~, an increase ~~in the amount~~ of weather perturbations due to ~~the~~ climate change, but also to urban developments in the
457 proximity of the stations, manufact building, vegetation growth, radio-electronic sources perturbations, traffic increase, etc.
458 In Fig. 11 we plot the RMS variation with time for some stations. A seasonal increase of the RMS is visible everywhere
459 throughout the considered time interval.

460



461

462 **Fig. 11: Variation of the RMS of the phase residuals with time of different GNSS stations.**

463

464

465

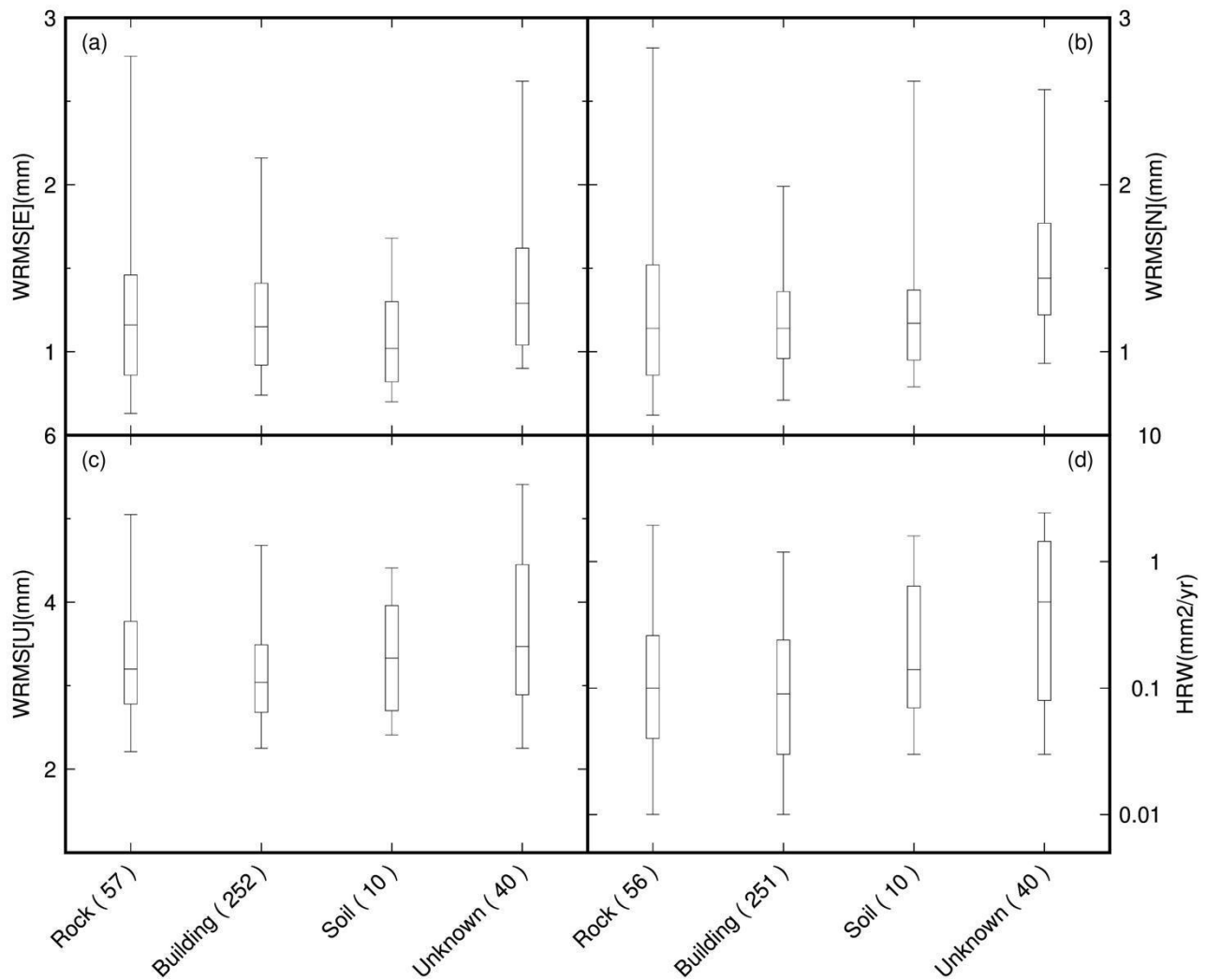
466 The phase RMS, typically 4-7 mm, increases up to 15-20 mm in July-August. This characteristic ~~regards whatever holds true~~
 467 ~~for any station, equally being whether it is~~ located near the coast (i.e., TRIE), ~~or~~ in the middle of the plain (as PAZO, PAVI)

468 or in a mountain context (i.e., ACOM, located at 1774 m altitude; MPRA, located at 808 m altitude; ZOUF, located at 1946
469 m altitude). The same also occurs at the stations in northern Europe; thus, it is a characteristic independent of the geographic
470 settingssetting. A crosscheck on the sky plots shows that the phase RMS increases particularly during the daytime. We suspect
471 it is due to variable-a mismodeling of the atmospheric noisedelay. We certainly know that data coming from sites in the tropics
472 haveare characterised by higher phase noise due to the higher water vapour content of the atmosphere. Orographic features
473 such as mountain ranges are prone to produce a highly-turbulent and asymmetric atmosphere, which is particularly
474 challenging to model. In other words, tropospheric asymmetries associated with topography, such as being on a mountain
475 range's windward or leeward side, can produce asymmetrical time series scatter due to local-scale weather conditions
476 (Materna, 2014).

477 Further considerations should be made for the MPRA station, which shows a systematic increase in the phase RMS since
478 2014. This condition is due to the construction of an electric tower in the proximity of the station, which has perturbed the
479 site's noise level, leading to increased uncertainties, evident in the station time series (see Appendix A). Also PAVI station
480 exhibits a systematically different RMS of the phase residuals since the second half of 2005, showing a decrease of ~ 2 mm.
481 This decrease is likely due to a change in the equipment. The Trimble Zephyr Geodetic antenna (TRM41249.00), on day
482 14/09/2005 was substituted by a Leica choke ring antenna (LEIAT504) which features superior multipath rejection with
483 uncompromised phase centre stability (<1mm) and is resistant to RF jamming ([http://uec-](http://uec-sigmat.com/Leica%20AT504%20(GG)%20Choke%20Ring%20Antenna%20-%20gps_gnss.html#productCollateralTabs1)
484 [sigmat.com/Leica%20AT504%20\(GG\)%20Choke%20Ring%20Antenna%20-%20gps_gnss.html#productCollateralTabs1](http://uec-sigmat.com/Leica%20AT504%20(GG)%20Choke%20Ring%20Antenna%20-%20gps_gnss.html#productCollateralTabs1)).
485 However, the phase RMS decrease is not so significant as of such magnitude to be reflectednoticeable in the uncertainty level,
486 or evident in the position time series of the site (see PAVI time series in the dataset).

487 Many authors have investigated the contribution of geodetic monuments to GNSS time series noise properties (e.g., Herring
488 et al., 2016; Langbein and Svarc, 2019 and reference therein). However, our dataset mainly comprises stations installed on
489 buildings, and each class of free-field installation (as defined in Fig. 5) consists of a limited number of stations. Therefore,
490 obtaininginferring reliable conclusions about the different free-field installation types is impossible. In Fig. 12, we compared
491 the noise properties of the time series (WRMS of the three components and HRW) of stations installed on buildings with
492 those of free-field installations. We conclude that the stations on buildings are not significantly different from the stations
493 installed on outcropping rocks.

494



495

496

497

498

499

Fig. 12: Box-and-whisker plots showing the distribution of the weighted-root-mean-square (WRMS) values estimated from the scatter of the station time series residuals along the East (a), North (b) and Up (c) components, and the equivalent horizontal random walk (HRW) represented the time-correlated noise. The line in the centre of the box is the median value, the boxes encompass 50% of stations (25th to 75th percentiles), the whiskers encompass 90% of stations (5th to 95th percentiles).

500

501

5.3 Comparison with previous works

502

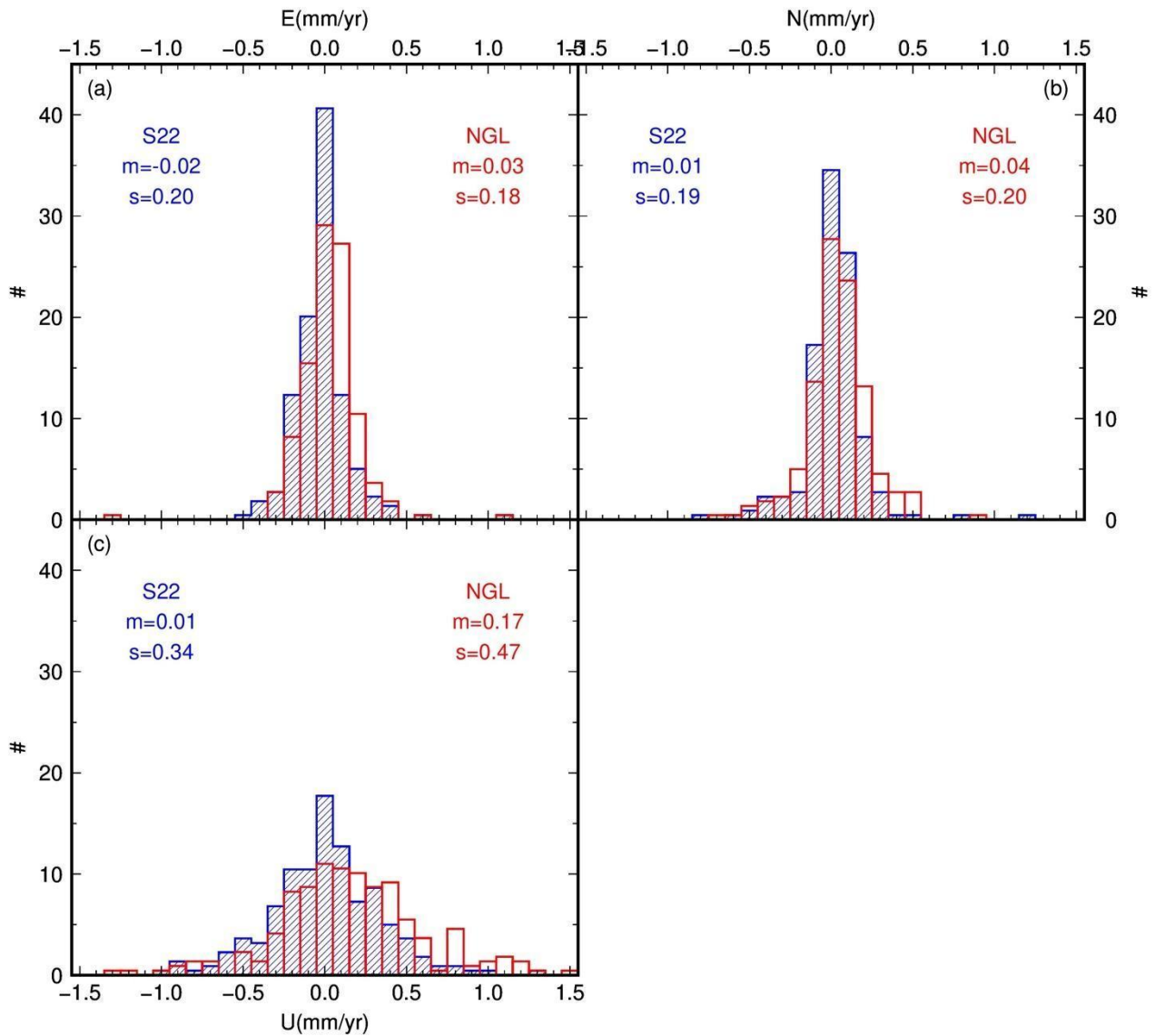
503

504

Different research groups published estimations of the velocity field in the area of interest of this study. Since the processing software or user-selected options can vary between different authors, through the comparison of our estimated velocities with those calculated by other researchers, we can evaluate the reliability of our solutions. If the misfits are not significant, we can

505 infer that our results are independent of data treatment and that our solutions are robust. On the contrary, if resulting velocities
506 are inconsistent between different studies, this can likely be ascribable to the differences in the data treatment performed. It
507 would be complicated to discriminate which research group has provided the best estimate of the velocity field.
508 We compared our results with those calculated by the Nevada Geodetic Laboratory (NGL), downloaded in the IGS14
509 reference frame from <http://geodesy.unr.edu/> on 2023, 3rd March, and by Serpelloni and co-workers, which recently
510 published the surface velocity of the Euro-Mediterranean region (Serpelloni et al., 2022). NGL uses the MIDAS software
511 (Blewitt et al., 2016) to estimate the velocity field and automatically estimate the time series trend, identifying step
512 discontinuities, outliers, seasonality and skewness in the data. Serpelloni and co-workers use the code of the Quasi
513 Observation Combination Analysis (QOCA) software developed by JPL (<https://qoca.jpl.nasa.gov>) to analyse the time series
514 and estimate the linear velocities. The comparison results are shown in Fig. 13 as histograms of solution differences. Overall,
515 the mean differences are ~~insignificant~~negligible, ranging from 0.01 mm/yr to 0.04 mm/yr in the horizontal component and to
516 0.01 mm/yr and 0.17 mm/yr in the vertical one, with the standard deviation ranging from 0.18 mm/yr to 0.47 mm/yr. Slightly
517 greater values are found ~~compared to~~in the comparison with the NGL solution, especially in the Up component. These low
518 discrepancies make us confident that our estimated velocities are robust and that the adopted data elaboration procedure is
519 effective.

520



521

522 **Fig. 13: Histograms of the differences between the velocity values estimated in this study, along the three components, and those**
 523 **estimated by Serpelloni and co-workers (S22, solution in blue colour) and by the Nevada Geodetic Lab (NGL, solution in red**
 524 **colour). Only the stations with a minimum of 4.5 years have been taken into consideration for the histograms.**

525

526

527 6 Data availability

528 The geodetic time series and velocity dataset is accessible ~~from the link~~
529 ~~https://frednet.crs.ogs.it/frednet_data/Projects/2022.OGS.GPS.solution/~~ on Zenodo (DOI 10.5281/zenodo.8055800) or from
530 the following DOI: ~~<https://doi.org/10.13120/b6aj-2s32>~~
531 ~~https://frednet.crs.ogs.it/frednet_data/Projects/2022.OGS.GPS.solution/~~ (Tunini et al., 2023). The products are distributed
532 under a Creative Common licence CC BY-SA. The time series for each GNSS station, covering the 2002-2022 time interval
533 (the last day processed is 2022, 30th June), are supplied in both international and Eurasia reference frames (ITRF14 and
534 ETRF14). Besides the GNSS time series plots, GAMIT/GLOBK pos-formatted files and ASCII formatted (Solution
535 INdependent Exchange - SINEX) daily files are provided. ~~Also, velocity~~ Velocity values are also provided in
536 international ITRF14 and Eurasia ETRF reference frames ~~(ITRF14 and ETRF14)~~,₂ and made available through tables and
537 ASCII-formatted SINEX files. An annual update of the estimated velocities is planned, while daily updated time series will
538 be available from the webpage <https://frednet.crs.ogs.it/DOI/> by clicking on the “solutions” link. Further related information
539 regarding the present paper (i.e., command files, information on jumps and discontinuities affecting the time series due to
540 earthquakes or equipment changes, station information, etc.) ~~are~~ is provided at the same link of the dataset.

541 7 Conclusions

542 This paper ~~documents the results of reports~~ the processing of two decades of continuous GNSS ~~observation~~
543 ~~regarding observations focused on~~ the ~~slowly~~ slowly convergent margin between the Eurasia plate and the Adria microplate.
544 ~~The dataset, available from the link~~ ~~https://frednet.crs.ogs.it/frednet_data/Projects/2022.OGS.GPS.solution/~~
545 ~~(<https://doi.org/10.13120/b6aj-2s32>)~~. The dataset, available on Zenodo (DOI 10.5281/zenodo.8055800), contains the
546 coordinate time series in both international and European reference frames, and velocity estimates for 350 permanent GNSS
547 stations belonging to different regional and international networks, covering a time interval from 2002-01-01 to 2022-06-30.
548 The time series are provided ~~cleaned-outpurged~~ of ~~unwanted~~ undesirable values, removed according to the following criteria:
549 (i) formal uncertainties; (ii) residuals concerning the RMS of the fit value and (iii) noise level. The estimated velocity values
550 ~~result~~ are retrieved from combining all the cleaned daily solutions.
551 Other research groups have also estimated consistent geodetic velocity values, but the corresponding time series are rarely
552 retrievable. Hence Therefore, the time series dataset presented here constitutes ~~a crucial~~ an important and complete source of
553 information about on the deformation of an active but ~~slowly~~ slowly converging margin ~~over~~ during the last two decades.
554 Furthermore In addition, the resulting time series are currently calculated and stored daily in the framework as part of a long-
555 term monitoring project, and ~~are always available from~~ can be accessed at any time via the webpage
556 <https://frednet.crs.ogs.it/DOI/>, ~~whereas~~ while the velocity solutions ~~are planned to~~ will be updated annually. An overview of
557 the employed-input data used, GNSS stations information and data processing strategy; is documented.

558 The original input data are RINEX-formatted ~~GNSS~~-daily GNSS observations, sampled every 30s and processed using the
559 GAMIT/GLOBK software package ~~ver10~~version 10.71. Data processing ~~has been~~was performed on the HPC cluster
560 GALILEO100 from CINECA, which uses the SLURM system for job scheduling and workload management. Different
561 experiments have been carried out on the same HPC cluster to evaluate the “goodness” of the applied processing procedure
562 ~~adopted~~ and the solidity of the solutions. The good results of the tests allow us to be confident that the dataset provided is
563 accurate and robust, and it can be used for high-precision deformation studies. In future studies, data from other GNSS
564 systems ~~data~~, such as Galileo or GLONASS observations, could also be included in the input data, ~~providing more to provide~~
565 further results and insights ~~on~~into the study region.

566

568 The Friuli Regional Deformation Network FReDNet (~~<http://frednet.crs.inogs.it/>~~ <https://frednet.crs.ogs.it>) is the OGS
 569 geodetic network established since the early 2000's in ~~the NE-Italy with the aim of monitoring~~. Its primary objective is to
 570 ~~monitor~~ the distribution of crustal deformation and ~~providing provide~~ supplementary information for the regional earthquake
 571 hazard assessment (Zuliani et al., 2018). First stations of FReDNet were installed in 2002. Since then, FReDNet has grown
 572 until counting, nowadays, 22 permanent GNSS stations covering homogeneously the eastern Alps, the alluvial plain and the
 573 coastal areas of NE-Italy (Fig. 1). Most of the time series are longer than 15 years (Table A1).

574

575 **Table A1. FReDNet stations specifics. MGBU station was installed on 2022, June 30th, therefore it is not included in the solution**
 576 **presented in the main text of the manuscript. UDIN is not operative anymore. H = hourly data sampled at 1s; D = daily data**
 577 **sampled at 30s; G = GLONASS satellites; R = RTK service; E = station belonging to EUREF Permanent Network (EPN) and data**
 578 **available from official EPN website <https://www.epncb.oma.be/networkdata/siteinfo4onestation.php?station=ZOUF00ITA>. Rock**
 579 **= site installed on hard terrain (not soil) or outcropping rocks. Building = site installed on a building or similar manufacts, like a**
 580 **wall, both on roof or fixed to the side wall. Soil = site installed on a soft terrain. *station name under definition; **dismissed in**
 581 **2006.**

	GNSS station	Antenna	Receiver	Operative since	Available services	Monument type	Location
1	ACOM	ASH701945E_M	TPS NET-G5	2003	H, D, G, R	concrete pillar with steel rods	Rock
2	AFAL	ASH701945E_M	TPS GB-1000	2003	H, D, G, R	concrete pillar with steel rods	Rock
3	CANV	ASH701945E_M	TPS NET-G5	2004	H, D, G, R	concrete pillar with steel rods	Rock
5	CODR	ASH701945E_M	TPS NET-G3A	2007	H, D, G, R	steel mast	Building
6	FUSE	ASH701945E_M	TPS NET-G5	2007	H, D, G, R	concrete pillar with steel rods	Rock
7	JOAN	ASH701945E_M	TPS NET-G5	2007	H, D, G, R	concrete pillar with steel rods	Rock
8	LODI*	TPSCR.G5	TPS NET-G5	2017	H, D, G	miscellaneous	Soil

9	MDEA	ASH701945E_M	TPS NET-G5	2003	H, D, G, R	concrete pillar with steel rods	Rock
10	MGBU	TPSCR.G5	TPS NET-G5	2022	H, D, G, R	concrete pillar with steel rods	Rock
11	MPRA	ASH701945E_M	TPS NET-G5	2002	H, D, G, R	concrete pillar with steel rods	Rock
12	NOVE	TPSCR3_GGD	TPS GB-1000	2009	H, D, G, R	steel mast	Soil
13	PAZO	TPSCR.G3	TPS NET-G3A	2007	H, D, G, R	steel mast	Soil
14	PMNT	TPSCR.G5	TPS NET-G3A	2015	H, D, G, R	steel mast	Rock
15	SUSE	TPSCR.G3	TPS NET-G3A	2011	H, D, G, R	concrete pillar with steel rods	Soil
16	TOLS	TPSCR.G5	TPS GB-1000	2021	H, D, G, R	steel mast	Building
17	TRIE	ASH701945E_M	TPS NET-G5	2003	H, D, G, R	steel mast	Building
18	UDI1	ASH701945E_M	TPS NET-G3A	2006	H, D, G, R	steel mast	Building
19	UDI2	LEIAR20	LEICA GR25	2010	H, D, G, R	steel mast	Building
--	UDIN**	ASH701975.01AGP	ASHTECH UZ-12	2002	H, D	steel mast	Building
20	VALS	TPSCR.G5	TPS NET-G5	2021	H, D, G, R	steel mast	Rock
21	VARM	TPSCR.G5	TPS NET-G5	2012	H, D, G, R	steel mast	Rock
22	ZOUF	ASH701945C_M	TPS GB-1000	2002	H, D, R, G, E	concrete pillar with steel rods	Rock

582

583

584

585 As mentioned in the main text, data from FReDNet are collected, quality-checked, transformed into the RINEX-formatted
586 data, and then released under a Creative Common licence (CC BY-SA), through a public ftp repository, as hourly and daily
587 files at both 1s and 30s sampling. The repository is the FReDNet Data Centre (FReDNet DC 2016) accessible at the link

588 <https://frednet.crs.ogs.it/DOI/>~~https://frednet.crs.ogs.it/DOI/~~, where also metadata of FReDNet sites (~~log sheets~~[sitelogs](#) in IGS
589 format) are available. Pictures of FReDNet stations are, instead, available on the FReDNet website

590 <http://frednet.crs.ogs.it/>~~https://frednet.crs.ogs.it/~~. FReDNet provides real-time data as well, through the Real Time
591 Kinematics (RTK) services, which allow reaching a centimetre-level accuracy in the positioning. The real-time data are
592 available, free of charge, through the NTRIP (Networked Transport of RTCM via Internet Protocol) distribution server.

593 Most of FReDNet stations are installed on solid rock or firmly monumented in the thick pebbly layer of the alluvial plain,
594 whereas 5 of them (CODR, TRIE, UDIN, UDI1, UDI2) are located on the roofs of small buildings. All the stations are
595 equipped with multi-frequencies and multi-constellations devices (Table A1). If the Topcon TPS GB-1000 and TPS NET-G3
596 receivers can track GPS and GLONASS satellite systems and just L1 and L2 frequency signals, the newest receivers TPS
597 NET-G5 are capable of tracking GPS, GLONASS, Galileo, and Beidou satellites and the signals L1, L2 and L5.

598 During the installation phase of FReDNet sites, particular attention had been paid to the site monument, which is crucial for
599 providing a stable and secure support for the antenna and hence for ensuring the good quality of the data retrieved. The
600 construction material should guarantee, within a reasonable low cost for building and maintenance, stability with time,

601 corrosion resistance, long term survivability, ~~zero~~[minimal](#) interaction with signal, resistance to frost action and temperature
602 variations, and ~~absence~~[low](#) or ~~minimum~~[negligible](#) amount of metal in the close proximity of the antenna. The site selected

603 for placing the monument should be easy accessible, clear of reflecting surfaces that can lead to multipath issues, with clear
604 horizon and controlled vegetation, and based on a shallow high quality bedrock with no local crust instabilities (cracks,
605 cavities, etc.). FReDNet sites were selected following the IGS recommendations, and periodically station maintenance is

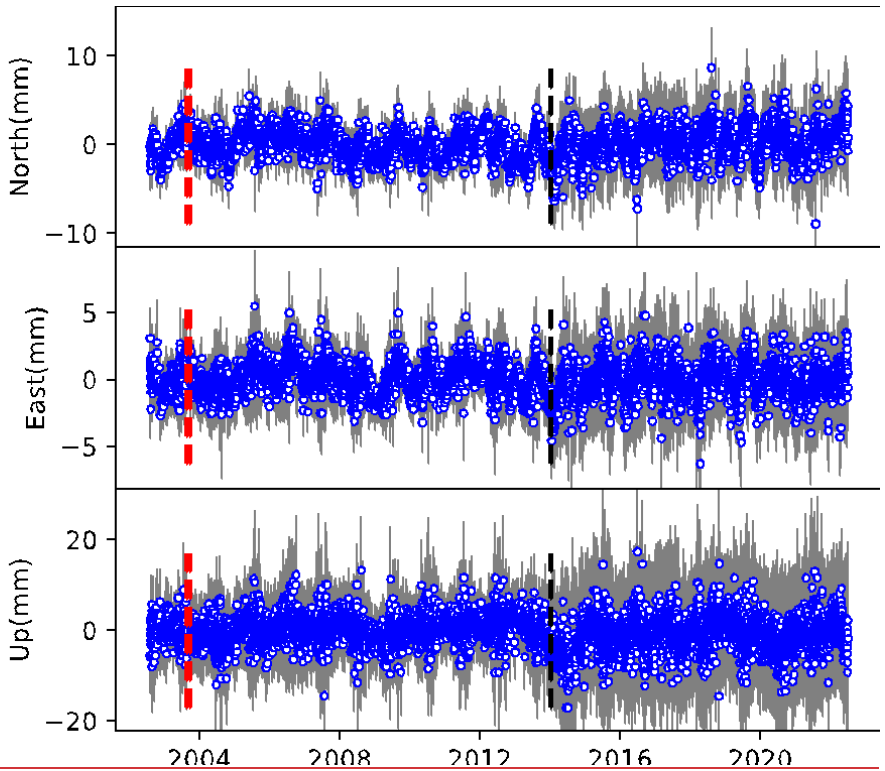
606 carried out to cut grown vegetation in proximity of the station or to restore the data connection. However, sometimes the
607 environment changes with no possibility of restoring the initial conditions. One example is MPRA station. Though the initial
608 location accomplished all the IGS requirements

609 (<https://files.igs.org/pub/station/general/IGS%20Site%20Guidelines%20July%202015.pdf>), in 2014 an electricity pylon was
610 built in the proximity of the station, with consequences on the background noise level, as evidenced by increased error bars

611 in the coordinate time series and in the phase RMS time series (Fig. A2). Nonetheless, our data processing strategy (illustrated
612 in Section 3 of the main text) allows us to retrieve a stable solution, even with the presence of noise time series as the one
613 provided by MPRA station.

614

615



616

617 **Fig. A1: MPRA station photo and time series of the residuals. Red dashed line indicates a change of the antenna, while black**
 618 **dashed line indicates the approximate date of the installation of the electricity pylon imaged in the photo.**

619

620 APPENDIX B. Daily local data processing

621 We implemented on a local machine the processing procedure described in the Section 3 of the main text with the aim to
 622 process the data following the 30th June of 2022. We have made the procedure automatic for daily processing. The local
 623 machine is a Mac mini equipped with Mac OS X (10.13) operative system. We use a crontab utility to manage the download
 624 of required input files, the update of metadata and the computation of daily solutions. From MIT, SOPAC, CDDIS and IGS
 625 repositories, we retrieve daily updates and files about orbits, atmospheric and tropospheric parameters, satellites aircrafts and
 626 ground station parameters, Earth orientation parameters, oceanic loading and tides, ionospheric and navigation files. RINEX
 627 files from FReDNet stations, EPOSA network and SLO_GPS stations are collected from OGS internal repositories.
 628 Observations from other networks are collected from the public data repositories of the networks, EPN data distribution
 629 services and EPOS service. ~~The download of the observations is~~ Observations are downloaded on a daily ~~made also~~
 630 searching basis, with a check for eventual missing observations in the 21 days before the processing date, in order to ~~remedy fix~~
 631 eventual data interruption or connectivity problems. Stations metadata are also downloaded periodically in the form of ~~log~~

632 [sheetssitelogs](#) from the public data repositories of the networks or from the M3G service and used to update the station
 633 information file and the file with the discontinuity.

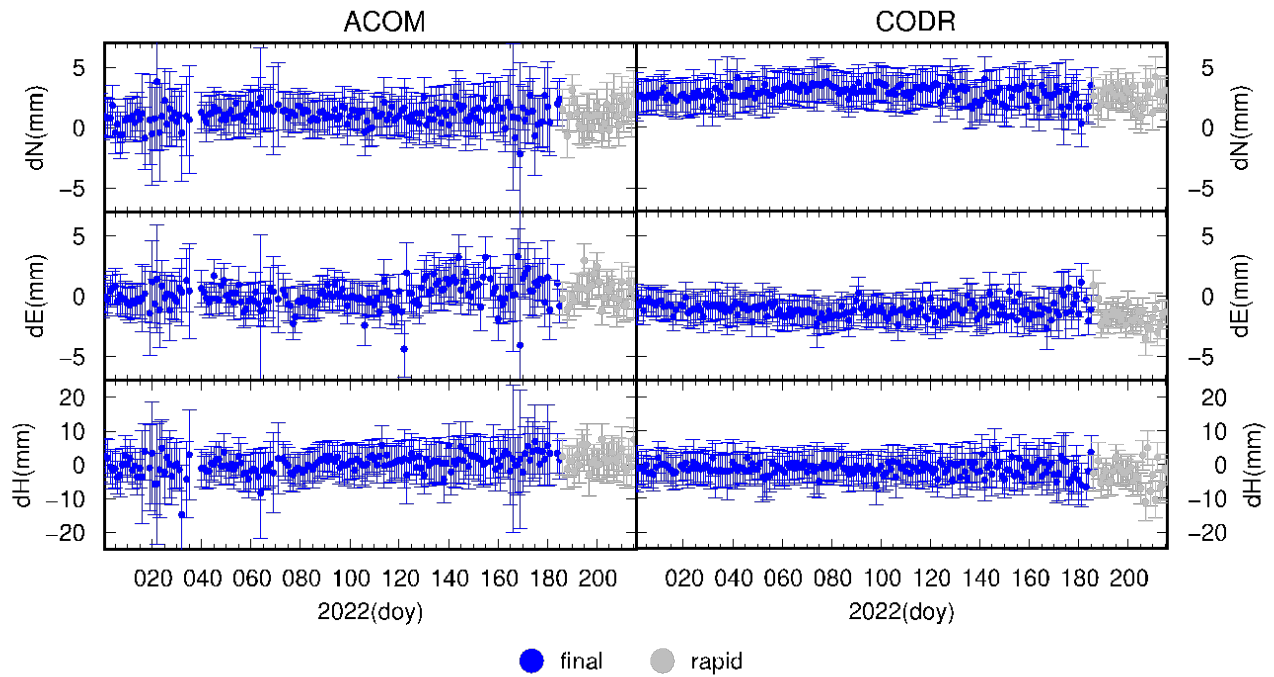
634 The automated procedure provides two types of time series for each GNSS station: i) coordinate time series obtained using
 635 IGS final orbit files (more precise) and ii) coordinate time series obtained using IGS rapid orbit files, which are less precise
 636 but available with just 3 days latency (https://cddis.nasa.gov/Data_and_Derived_Products/GNSS/orbit_products.html). In
 637 particular, coordinate time series are calculated using final orbit files until 30 days before the processing date, and using rapid
 638 orbit files until 3 days before the processing date. An example of the resulting time series is given in Fig. B1.

639 Once the daily processing is finalized, an automatic e-mail message is sent to the data analysts with the summary of the
 640 processing results.

641 Finally, a periodic download of the latest tar-file containing incremental updates for GAMIT/GLOBK software is planned, in
 642 order to keep the software updated. We ~~also plan~~ to update the velocity solution each year.

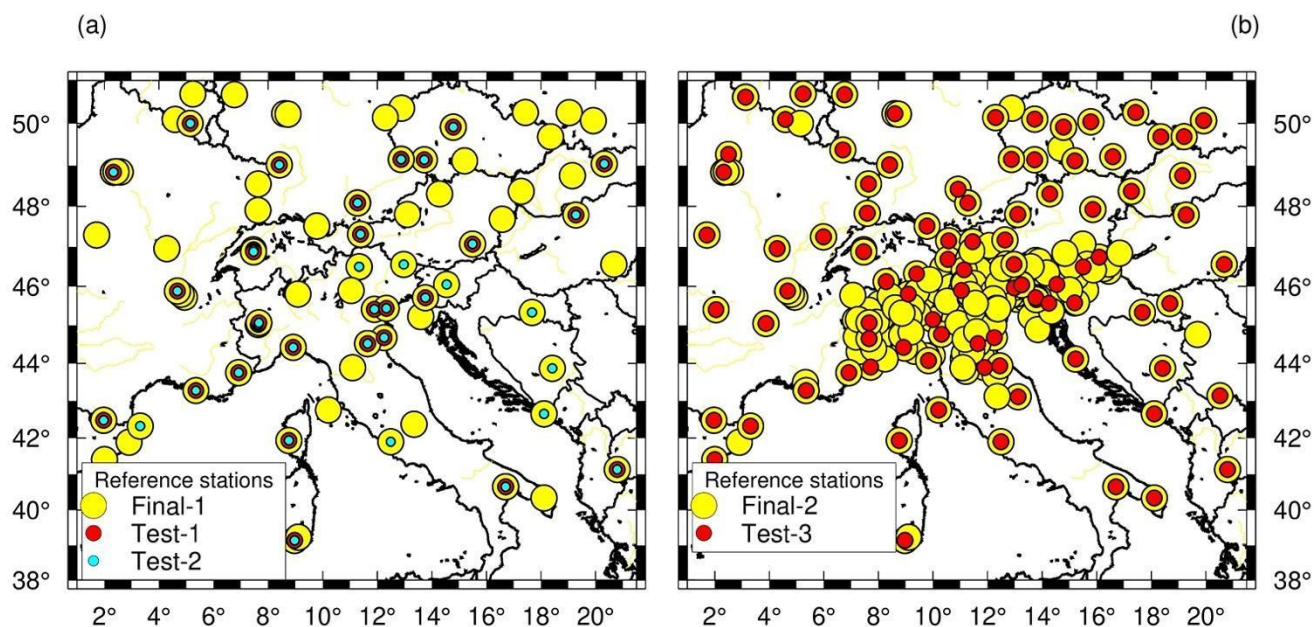
643

644



645

646 **Fig. B1:** Coordinate time series in ETRF14 reference frame, calculated using final orbits (blue symbols) and rapid orbits (grey
 647 symbols). Example for ACOM and CODR stations covering the time interval 2022-01-01/2022-08-04.
 648



650

651 **Fig. C1: Reference sites used in the tests (Test-1, Test-2, Test-3) illustrated in Section 5.1, plotted as red and cyan circles,**
 652 **compared to the reference sites used in the final processing (Final-1 and Final-2 indicate the first and second iteration,**
 653 **respectively, of the velocity calculation explained in Section 3), plotted as yellow circles.**

654

655 Author contributions

656 DZ, GR, AM, LT developed the concept of this work. DZ developed the FReDNet network with the contribution of OGS
 657 technical staff, and he set up the real-time data distribution service. AM, LT processed and elaborated the dataset, and prepared
 658 the manuscript and the figures. AM, LT, GR, DZ reviewed and edited the manuscript. All the authors have read and approved
 659 the submitted manuscript.

660 Competing interests

661 The authors declare that they have no conflict of interest.

662 Acknowledgements

663 This research was supported by OGS and CINECA under HPC-TRES program award number 2020-11. We acknowledge the
 664 CINECA award under the ISCRA initiative, for the availability of high performance computing resources and support (IscraC

665 IsC83_GPSIT and IsC96_GPSIT-2 projects). FReDNet is managed by OGS with support of the FVG Regional Civil
666 Protection. We thank OGS staff for their support with the maintenance of the FReDNet GNSS network. We are grateful to
667 all public and private institutions that made the continuous GPS data used in this work available. We thank [Pavel Kosovac](#)
668 [and Dusko Vranac from Zavod MPRI, raziskovalna in razvojna dejavnost, the University of Ljubljana](#), the GAMIT/GLOBK
669 team at MIT for their continuous support, [and two anonymous reviewers for their constructive comments and considerations](#).
670 All figures have been made using the GMT software (Wessel et al., 2019), except for Fig. 4 made with PowerPoint
671 (<https://www.microsoft.com/it-it/microsoft-365/powerpoint>) and for Fig. A1 made with Matplotlib (Hunter, 2007).
672 Information on GMT can be found at: <https://www.generic-mapping-tools.org/>, information on GNSMART can be found at:
673 <https://www.geopp.de/gnsmart/>, information on GAMIT/GLOBK can be found at: <http://geoweb.mit.edu/gg/>.

674 **References**

- 675 Alken, P., Thébaud, E., Beggan, C.D. Amit, H, Aubert, J., Baerenzung, J., Bondar, T.N., Browin, W.J., Califf, S., Chambodut,
676 A., Chulliat, A., Cox, G.A., Finlay, C.C., Fournier, A., Gillet, N., Grayver, A., Hammer, M.D., Holschneider, M., Huder, L.,
677 Hulot, G., Jager, T., Kloss, C., Korte, M., Kuanh, W., Kuvshinov, A., Langlais, B., Léger, J.-M., Levur, V., Livermore, P.W.,
678 Lowes, F.J., Macmillan, S., Magnes, W., Manda, M., Marsal., S., Matzka, J., Metman, M.C., Minami, T., Morschhauser, A.,
679 Mound, J.E., Nair, M., Nakano, S., Olsen, N., Pavón-Carrasco, F.J., Petrov, V.G., Ropp, G., Rother, M., Sabaka, T.J.,
680 Sanchez, S., Saturnino, D., Schnepf, N.R., Shen, X., Stolle, C., Tangborn, A., Tøffner-Clausen, L., Tob, H., Torta, J.M.,
681 Varner, J., Vervelidou, F., Vigneron, P., Wardinski, I., Wicht, J., Woods, A., Yang, Y., Zeren, Z., and Zhou, B.: International
682 Geomagnetic Reference Field: the thirteenth generation. *Earth Planets Space* 73, 49, [doi: 10.1186/s40623-020-01288-x](https://doi.org/10.1186/s40623-020-01288-x), 2021.
683
- 684 Altamimi, Z., Rebischung, P., Métivier, L., and Collilieux, X.: ITRF2014: A new release of the International Terrestrial
685 Reference Frame modeling nonlinear station motions, *J. Geophys. Res. Solid Earth*, 121, [doi:10.1002/2016JB013098](https://doi.org/10.1002/2016JB013098), 2016.
686
- 687 Altamimi, Z., Métivier, L., Rebischung, P., Rouby, H., Collilieux, X.: ITRF2014 plate motion model, *Geophysical Journal*
688 *International*, 209(3),1906–1912, [doi:10.1093/gji/ggx136](https://doi.org/10.1093/gji/ggx136), 2017.
689
- 690 Amante, C., and Eakins, B. W. (2009). ETOPO1 1 Arc-Minute Global Relief Model: Procedures, Data Sources and
691 Analysis. NOAA Technical Memorandum NESDIS NGDC-24. Silver Spring: NOAA.
692
- 693 Battaglia, M., Zuliani, D., Pascutti, D., Michelini, A., Marson, I., Murray, M.H., Burgmann, R.: Network Assesses Earthquake
694 Potential in Italy's Southern Alps, *EOS*, 84, 262–264, 2003.
695
696

697 Blewitt, G, and Lavallee, D.: Effect of annual signals on geodetic velocity, *J. Geophys. Res.*, 107 (B7), 2002.
698

699 Blewitt, G., Kreemer, C., Hammond, W.C., and Gazeaux J.: MIDAS robust trend estimator for accurate GPS station velocities
700 without step detection, *Journal of Geophysical Research*, 121, doi:10.1002/2015JB012552, 2016.
701

702 [Blewitt, G., W. C. Hammond, and C. Kreemer: Harnessing the GPS data explosion for interdisciplinary science, *Eos*, 99,](https://doi.org/10.1029/2018EO104623)
703 [https://doi.org/10.1029/2018EO104623, 2018.](https://doi.org/10.1029/2018EO104623)
704

705 Boehm, J., Werl, B., and Schuh, H.: Troposphere mapping functions for GPS and very long baseline interferometry from
706 European Centre for Medium-Range Weather Forecasts operational analysis data.
707 doi:[10.1029/2005JB003629](https://doi.org/10.1029/2005JB003629):[10.1029/2005JB003629](https://doi.org/10.1029/2005JB003629), 2006a.
708

709 Boehm, J., Niell, A., Tregoning, P., and Schuh, H.: Global mapping function (GMF): a new empirical mapping function based
710 on numerical weather model data *Geophys. Res. Lett.* 33, 2006b.
711

712 Bragato, P. L., Comelli, P., Sara, A., Zuliani, D., Moratto, L., Poggi, V., Rossi, G., Scaini, C., Sugan, M., Barnaba C.,
713 Bernardi, P., Bertoni, M., Bressan, G., Compagno, A., Del Negro, E., Di Bartolomeo, P., Fabris, P., Garbin, M., Grossi, M.
714 Magrin, A., Magrin, E., Pesaresi, D., Petrovic, B., Plasencia Linares, M.P., Romanelli, M., Snidarcig, A., Tunini, L., Urban,
715 S., Venturini, E., Parolai, S.: The OGS - Northeastern Italy seismic and deformation network: Current status and outlook,
716 *Seismol. Res. Lett.* 92, no. 3, 1704–1716, doi:[10.1785/0220200372](https://doi.org/10.1785/0220200372), 2021.
717

718 Braitenberg, C., and Zadro, M.: The Grotta Gigante horizontal pendulums - instrumentation and observations. *Bollettino di*
719 *Geofisica Teorica e Applicata*, 40(3/4), 577–582, 1999.
720

721 Brancolini, G., Civile, D., Donda, F., Tosi, L., Zecchin, M., Volpi, V., Rossi, G., Sandron, D., Ferrante, G.M., and Forlin, E.:
722 New insights on the Adria plate geodynamics from the northern Adriatic perspective, *Marine and Petroleum Geology*, 109,
723 687-697, 2019.
724

725 Bressan, G., Barnaba, C., Peresan, A., & Rossi, G. Anatomy of seismicity clustering from parametric space-time analysis.
726 *Physics of the Earth and Planetary Interiors*, 320, 106787, 2021.
727

728 Castellarin, A., & Cantelli, L.: Neo-Alpine evolution of the southern Eastern Alps. *Journal of Geodynamics*, 30(1-2), 251-
729 274, 2000.
730

731 D'Agostino, N., Avallone, A., Cheloni, D., D'Anastasio, E., Mantenuto, S., and Selvaggi, G.: Active tectonics of the Adriatic
732 region from GPS and earthquake slip vectors. *J. Geophys. Res.* 113:B12413. doi: 10.1029/2008JB005860, 2008.

733

734 D'Agostino, N., Cheloni, D., Mantenuto, S., Selvaggi, G., Michelini, A., and Zuliani, D.: Strain accumulation in the southern
735 Alps (NE Italy) and deformation at the northeastern boundary of Adria observed by CGPS measurements. *Geophys. Res.*
736 *Lett.* 32:L19306. doi:10.1029/2005GL024266, 2005.

737

738 Devoti, R., Esposito, A., Pietrantonio, G., Pisani, A. R., and Riguzzi, F.: Evidence of large scale deformation patterns from
739 GPS data in the Italian subduction boundary. *Earth and Planetary Science Letters*, 311(3-4), 230-241, 2011.

740

741 Dong, D., Herring, T. A., and King, R. W.: Estimating Regional Deformation from a Combination of Space and Terrestrial
742 Geodetic Data. *J. Geodesy* 72 (4), 200–214. doi:10.1007/s001900050161, 1998.

743

744 Estey, L.H. and Meertens, C.M.: TEQC: The Multi-Purpose Toolkit for GPS/GLONASS Data and GPS Solutions; John Wiley
745 & Sons: New York, NY, USA, Volume 3, pp. 42–49, 1999.

746

747 Floyd, M. A., and Herring, T. A.: Fast statistical approaches to geodetic time series analysis. In J. P. Montillet & M. Bos
748 (Eds.), *Geodetic Time Series Analysis in Earth Sciences* Bos and Montillet, Springer Geophysics. Cham: Springer.
749 doi:[10.1007/978-3-030-21718-1](https://doi.org/10.1007/978-3-030-21718-1), 2019.

750

751 Floyd, M. A., Billiris, H., Paradissis, D., Veis, G., Avallone, A., Briole, P., McClusky, S., Nocquet, J.M., Palamartchouk, K.,
752 Parsons, B., and England, P. C.: A new velocity field for Greece: Implications for the kinematics and dynamics of the Aegean,
753 *J. Geophys. Res.*, 115, B10403, doi:10.1029/2009JB007040, 2010.

754

755 FReDNet DC: Friuli Regional Deformation Network Data Center. Istituto Nazionale di Oceanografia e Geofisica
756 Sperimentale, Dataset, doi:10.6092/frednet, 2016.

757

758 Gerhard, W., Andreas, B., Martin, S.: RTK Networks based on Geo++ ® GNSMART—Concepts, Implementation, Results.
759 In *Proceedings of the International Technical Meeting (ION GPS-01)*, Salt Lake City, UT, USA, 11–14 September 2001.

760

761 Herring, T. A., Melbourne, T. I., Murray, M. H., Floyd, M. A., Szeliga, W. M., King, R. W., ... & Wang, L.: Plate Boundary
762 Observatory and related networks: GPS data analysis methods and geodetic products, *Reviews of Geophysics*, 54(4), 759-
763 808, 2016.

764
765 Herring, T.A., King, R.W., Floyd, M.A., and McClusky, S.C.: Introduction to GAMIT/GLOBK Introduction to
766 GAMIT/GLOBK, Release 10.7. Available at: http://geoweb.mit.edu/gg/docs/Intro_GG.pdf, 2018.

767
768 Hunter, J. D. : Matplotlib: A 2D Graphics Environment, Computing in Science & Engineering, vol. 9, no. 3, pp. 90-95, 2007.

769
770 [Johnston, G., Riddell, A., Hausler, G.: The International GNSS Service. Teunissen, Peter J.G., & Montenbruck, O. \(Eds.\),](#)
771 [Springer Handbook of Global Navigation Satellite Systems \(1st ed., pp. 967-982\). Cham, Switzerland: Springer International](#)
772 [Publishing. DOI: 10.1007/978-3-319-42928-1, 2017.](#)

773
774 [Labib, B., Yan, J., Barriot, J. P., Zhang, F., & Feng, P.: Monitoring Zenithal Total Delays over the three different climatic](#)
775 [zones from IGS GPS final products: A comparison between the use of the VMF1 and GMF mapping functions. Geodesy and](#)
776 [Geodynamics, 10\(2\), 93-99, 2019.](#)

777
778 Langbein, J., and Svarc, J. L.: Evaluation of temporally correlated noise in Global Navigation Satellite System time series:
779 Geodetic monument performance. Journal of Geophysical Research: Solid Earth, 124(1), 925-942, 2019.

780
781 [Lyard, F., Lefevre, F., Letellier, T., & Francis, O.: Modelling the global ocean tides: modern insights from FES2004. Ocean](#)
782 [dynamics, 56, 394-415, 2006.](#)

783
784 Magrin, A., and Rossi, G.: Deriving a new crustal model of Northern Adria: The Northern Adria Crust (NAC) Model.
785 Frontiers of Earth Science, 8, doi:[10.3389/feart.2020.00089](https://doi.org/10.3389/feart.2020.00089), 2020.

786
787 Masson, C., Mazzotti, S., Vernant, P.: Precision of continuous GPS velocities from statistical analysis of synthetic time series,
788 Solid Earth, 10: 329–342, <https://doi.org/10.5194/se-10-329-2019>, 2019.

789
790 [Materna, K.: Analysis of atmospheric delays and asymmetric positioning errors in the global positioning system \(Doctoral](#)
791 [dissertation, Massachusetts Institute of Technology\), 2014.](#)

792
793 Matthews, K. J., Maloney, K. T., Zahirovic, S., Williams, S. E., Seton, M., and Müller, R. D.: Global plate boundary evolution
794 and kinematics since the late Paleozoic: Global and Planetary Change, doi:[10.1016/j.gloplacha.2016.10.002](https://doi.org/10.1016/j.gloplacha.2016.10.002), 2016.

795

796 [Noll, C.: The Crustal Dynamics Data Information System: A resource to support scientific analysis using space geodesy,](#)
797 [Advances in Space Research, Volume 45, Issue 12, 15 June 2010, Pages 1421-1440, ISSN 0273-1177, DOI:](#)
798 [10.1016/j.asr.2010.01.018, 2010.](#)
799

800 Petit, G. and Luzum, B.: IERS conventions, Tech. rep., Bureau International des Poids et mesures sevres (France), 2010.
801

802 Priolo, E., Zinno, I., Guidarelli, M., Romanelli, M., Lanari, R., Sandron, D., Garbin, M., Peruzza, L., Romano, A., Zuliani,
803 D., Tunini, L., Magrin, A: The birth of an underground gas storage in a depleted gas reservoir - Results from integrated
804 seismic and ground deformation monitoring, under review.
805

806 Rossi, G., Pastorutti, A., Nagy, I., Braitenberg, C., and Parolai, S.: Recurrence of Fault Valve Behavior in a Continental
807 Collision Area: Evidence From Tilt/Strain Measurements in Northern Adria, *Frontiers in Earth Science*, 9, 641416, 2021.
808

809 Serpelloni, E., Anzidei, M., Baldi, P., Casula, G., and Galvani, A.: Crustal velocity and strain-rate fields in Italy and
810 surrounding regions: new results from the analysis of permanent and non-permanent GPS networks, *Geophys. J. Int.* 161,
811 861–880, doi: 10.1111/j.1365-246X.2005.02618.x, 2005.
812

813 Serpelloni, E., Cavaliere, A., Martelli, L., Pintori, F., Anderlini, L., Borghi, A., Randazzo, D., Bruni, S., Devoti, R., Perfetti,
814 P., and Cacciaguerra, S.: Surface Velocities and Strain-Rates in the Euro-Mediterranean Region From Massive GPS Data
815 Processing, *Front. Earth Sci.*, 10, 1–22, 2022.
816

817 [Steigenberger, P., Boehm, J., & Tesmer, V.: Comparison of GMF/GPT with VMF1/ECMWF and implications for](#)
818 [atmospheric loading. *Journal of Geodesy*, 83, 943-951, 2009.](#)
819

820 Tunini, L., Magrin, A., Rossi, G., Zuliani, D.: GNSS time series and velocities about a slow convergent margin processed on
821 HPC clusters: products and robustness evaluation [data set], <https://doi.org/10.13120/b6aj-2s32>—DOI
822 [10.5281/zenodo.8055800](https://doi.org/10.5281/zenodo.8055800), 2023.
823

824 U.S.G.S., US Geological Survey, Earthquake Hazards Program: Advanced National Seismic System (ANSS) Comprehensive
825 Catalog of Earthquake Events and Products: Various, <https://doi.org/10.5066/F7MS3QZH>, 2017.
826

827 Weber, J., Vrabec, M., Pavlovčič-Prešeren, P., Dixon, T., Jiang, Y., and Stopar, B.: GPS-derived motion of the Adriatic
828 microplate from Istria Peninsula and Po Plain sites, and geodynamic implications. *Tectonophysics*, 483(3-4), 214-222, 2010.
829

830 Wessel, P., Luis, J. F., Uieda, L., Scharroo, R., Wobbe, F., Smith, W. H. F., & Tian, D.: The Generic Mapping Tools version
831 6. *Geochemistry, Geophysics, Geosystems*, 20, 5556–5564. <https://doi.org/10.1029/2019GC008515>, 2019.
832
833 Zuliani, D., Fabris, P., Rossi, G.: FReDNet: Evolution of permanent GNSS receiver system. In: *New Advanced GNSS and
834 3D Spatial Techniques Applications to Civil and Environmental Engineering, Geophysics, Architecture, Archeology and
835 Cultural Heritage, Lecture Notes in Geoinformation and Cartography*; Cefalo, R., Zielinski, J., Barbarella, M., Eds.; Springer:
836 Cham, Switzerland, pp.123–137, 2018.